# Infrared Spectra and Density Functional Theory Calculations on Transition Metal Nitrosyls. Vibrational Frequencies of Unsaturated Transition Metal Nitrosyls

Lester Andrews* and Angelo Citra

*University of Virginia, Department of Chemistry, P.O. Box 400319, Charlottesville, Virginia 22904-4319*

*Received April 17, 2001*

## *Contents*



## *I. Introduction*

Although the chemistry of nitric oxide is extremely important in several areas of chemistry, the interaction of NO with transition metals is perhaps the most noteworthy. The reaction of nitric oxide on metal surfaces and in contact with metal cations in zeolites is important in the development of effective catalysts that can reduce atmospheric pollution.[1−3] The susceptibility of adsorbed NO to dissociation on metal substrates depends on the metal position in the periodic table, which relates to the heat of adsorption.[1] In addition, transition metal (TM) nitrosyl complexes play many roles. Novel nitrosyl structures may form the basis for information storage by virtue of long-lived metastable isomers.[4−7] Furthermore, the interaction of nitric oxide with TM centers in biological systems has also received considerable attention as the large number of such reviews included in this special NO issue demonstrates. Nitric oxide binds to the heme center in metalloproteins and has been identified as an important messenger molecule in neurophysical systems.[8−11] Finally, nitric oxide reacts with superoxide to form peroxynitrite, which has serious pathological consequences in the human system.[12]

At the heart of these research areas is the fundamental interaction between NO and transition metal atoms. In the past this has been classified in terms of the electron count in the {MNO} subunit in larger complexes, and qualitative molecular orbital diagrams have been constructed to explain and predict the properties of such compounds.[13] While these schemes are useful, they have been surpassed by quantum chemical calculations, in particular density functional theory (DFT), that can compute the equilibrium and associated properties of TM nitrosyl containing species, including metal nitrosyl complexes,[14,15] and even first principles calculations for nitric oxide on extended metal surfaces.[16] Such calculations do away with the assumptions of early bonding models and introduce a number of new parameters to characterize a nitrosyl complex or an extended system, namely the structure, energy, and nitrosyl stretching frequencies. The experimental measurement and DFT calculation of simple binary TM nitrosyl vibrational frequencies is the subject of this review.

The fundamental interaction between TM atoms and nitric oxide is explored using the matrix-isolation technique to react NO with transition metal atoms, to trap the product complexes, and to observe their infrared spectra. The matrix-isolation method allows the formation of small unsaturated binary transition metal nitrosyls without additional ligands that may complicate the chemistry and the spectrum. These unsaturated fragments are kinetically stabilized in solid argon or neon at cryogenic temperatures; subsequent annealing softens the matrix and allows trapped species to diffuse and to interact with each other, and after several annealing cycles, the full range of nitrosyl complexes of a given metal can be observed. Irradiation of the matrix with ultraviolet (UV) light promotes photochemistry of trapped species. The observed TM nitrosyl infrared absorption

10.1021/cr0000729 CCC: $39.75 
Published on Web 03/15/2002

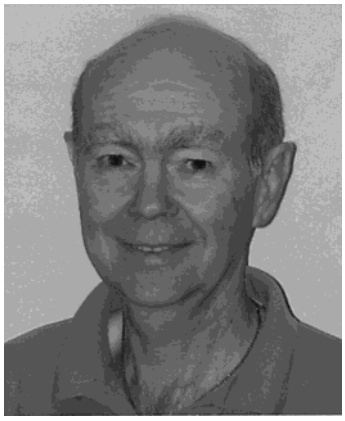

Lester Andrews was born in Lincolnton, NC, on January 31, 1942. He earned a B.S. degree in Chemical Engineering from Mississippi State University in 1963 and a Ph.D. degree in Physical Chemistry from the University of California, Berkeley, in 1966. Dr. Andrews joined the faculty of the University of Virginia in 1966 where he has been active in matrix-isolation spectroscopy, publishing over 550 research papers on novel chemical species. Otherwise, he enjoys white-water canoeing and playing the clarinet.

Angelo Citra was born in London, England, in 1973. He was educated in state schools. He received his MChem degree from the University of Southampton in 1996 and his Ph.D. degree from the University of Virginia in 2001. For relaxation, he plays chess and the guitar.

profiles will be compared with the results of DFT frequency calculations from the last 10 years. This provides a means to verify experimental assignments and allows the effectiveness of the various density functionals to be directly assessed. The careful selection of reaction conditions allows positively and negatively charged species to be observed in addition to neutral complexes, and this facilitates an estimate of the effective charge in nitric oxide adsorbed to supported metal surfaces and complexed to metal centers in physiological systems.

Although the matrix-isolation technique has provided much valuable spectroscopic information on coordinatively unsaturated TM carbonyls over the last three decades,[17−22] this method has only been recently applied to the study of unsaturated TM nitrosyls. Ball and co-workers[23−25] reported the first observations of late first-row TM nitrosyls in 1994−1996, our team investigated the $Cr(NO)_{1,2,3,4}$ and $Mn(NO)_{1,2,3}$ systems in 1998,[26,27] and the Manceron group followed with several nickel nitrosyl species the next year.[28] The above studies have characterized the expected $\eta^1$-NO end-bound nitrosyls, the novel $\eta^2$-NO side-bound species, and the unexpected NMO nitride-oxide insertion products. These three products vary in relative stability across the periodic table as will be described here.

The only stable binary TM nitrosyl, $Cr(NO)_4$, was examined in solid matrices over 20 years ago, but attempts to photodissociate this precursor into unsaturated intermediate species as done for the analogous stable carbonyl,[17] $Cr(CO)_6$, gave only a metastable $Cr(NO)_3(NO)^*$ species where (NO)* denotes a different bonding arrangement.[29] Several saturated mixed carbonyl nitrosyls have been irradiated,[30−32] but the products have been identified as mixed carbonyl nitrosyls of the type formed recently from the metal atoms, CO, and NO during condensation in excess argon.[33−35] However, in the case of $Mn(NO)_3(CO)$, the loss of CO gave $Mn(NO)_3$ as will be discussed below.

We will review here experiments to synthesize simple MNO compounds and to trap them for measurement of nitrosyl vibrational frequencies and DFT calculations of those same nitrosyl vibrational frequencies.

## II. Experimental and Theoretical Methods

### A. Sample Preparation

The synthesis of unsaturated transition metal (TM) nitrosyl species is the first step for spectroscopic study. Since $Cr(NO)_4$ is the only stable TM nitrosyl,[36] the only general method available is the direct synthesis from metal atoms and NO; see reaction 1 with $x$ depending on the metal electron count.

$$M + xNO \rightarrow M(NO)_x \quad (x = 1, 2, 3, 4) \qquad (1)$$

The conventional method for producing TM atoms is thermal evaporation from high-current filament sources as employed by the Ball and Manceron groups.[23−25,28] Advantages of this method are that the atom energies are thermal, the radiation background is minimal, and high atom fluxes can be generated.

Another technique to produce metal atoms is laser ablation. This method has been recently employed in our laboratory to synthesize unsaturated transition metal nitrosyls in rare gas matrices.[26,27] Laser ablation has proven to be a powerful method to produce reactive intermediates and radicals for gas-phase jet studies as well as lower temperature matrix-isolation investigations.[37] A schematic diagram of a reactive laser-ablation apparatus for matrix-isolation infrared spectroscopic investigation of unsaturated transition metal nitrosyl species is shown in Figure 1, and the experimental procedure has been described earlier.[20−22,38,39] The cold window is maintained at 10 K (model 22 Cryocooler, CTI Cryogenics, Waltham, MA) or 7 K (Displex, APD Cryogenics, Allentown, PA) for argon matrix studies or at 4 K (Heliplex, APD Cryogenics, Allentown, PA) for neon matrix investigations. Laser ablation has a number of advantages in comparison to conventional high-temperature oven techniques. With the laser-ablation technique, only a small amount of the material is directly heated, thus minimizing the

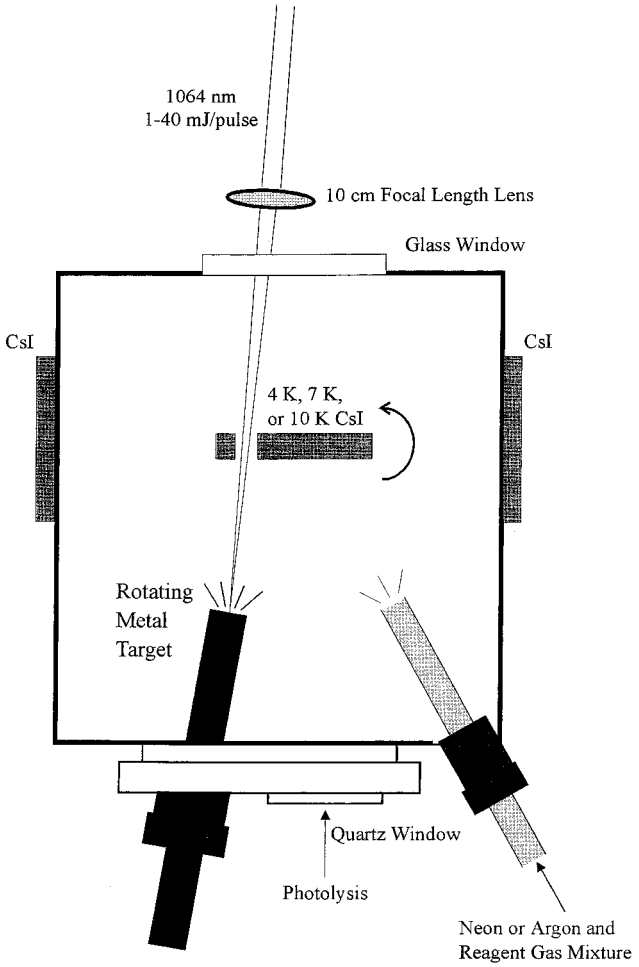


**Figure 1.** Schematic diagram of apparatus for laser-ablation matrix-isolation infrared spectroscopic investigation of unsaturated transition metal nitrosyls. After sample deposition, the cold window is rotated 90° to record spectra.

heat load on the cold matrix and the introduction of impurities into the sample. Of more importance, laser ablation produces electrons and cations as well as neutral atoms, and as a result, anions can be formed by electron capture of the neutral molecules, and cations can be produced by cation−molecule reactions or via photoionization by radiation in the ablation plume. The most obvious disadvantage of laser ablation is the plume of radiation produced by laser excitation of the target material; thus, the samples are deposited with concurrent irradiation. Recently, a large number of new unsaturated transition metal nitrosyl neutrals, cations, and anions have been produced in our laboratory upon reactive co-condensation of laser-ablated transition metal atoms, cations, and electrons with NO in excess argon or neon, and these investigations will be discussed here.

Quartz-crystal microbalances are often used to measure the amount of metal deposited in matrix-isolation experiments.[18,19] The present experiments employed 1−40 mJ per10 ns pulse of 1064 nm radiation focused (10 cm f.l.) on the rotating metal target. Microbalance measurements provide a basis to estimate the metal mole concentration as 0.1% of the argon matrix (this can range from 0.2% to 0.02% in different experiments, but the metal concentration is always less than the NO concentration). Typically laser-ablation experiments employ lower metal concentrations than thermal evaporation experiments.[19,22,40] The neon matrix experiments included a 10% neutral density filter in the laser beam with the same laser focus, and microbalance measurements typically found 15% as much metal ablated. The metal mole concentrations in the neon matrix experiments discussed here are therefore approximately 0.02% of the neon matrix (range from 0.03 to 0.01%).

One problem in spectroscopic studies of transition metal nitrosyls is the unambiguous identification of the observed spectral features. With isotopic substitution and isotopic mixtures, the composition can be established, but the real difficulty usually lies in the correct identification of charged species. Some information about charge can be obtained from photolysis behavior. Unsaturated transition metal nitrosyls are expected to have small electron affinities (less than 3 eV), and visible or ultraviolet photolysis can easily detach the anion electron, but the cations are usually more strongly bound. However, electrons detached from anions may then neutralize cations. Of more importance, many neutral unsaturated transition metal nitrosyl species are photosensitive, and charge state identification via photolysis behavior is not reliable. When cations and electrons are present, more information about charge state can be obtained from electron trap molecule (such as $CCl_4$) doping experiments. The role of $CCl_4$ as an electron trap in laser-ablation experiments has been discussed by Zhou and Andrews in a series of cation and anion studies.[20,21,40−42] Laser ablation of the metal target produces metal atoms, metal cations, and electrons, and the added $CCl_4$ captures most of the ablated electrons that reach the sample, thus reducing the yield of molecular anions and facilitating the survival of more laser-ablated metal cations and their reaction products. The $CCl_4$ doping technique has been employed to aid in the identification of TM nitrosyl cations and anions.

## B. Spectroscopic Methods

Infrared absorption is the main spectroscopic method used to characterize coordinatively unsaturated TM nitrosyls. Fortunately, these molecules exhibit strong absorptions in the N−O stretching vibrational region that are often both stoichiometrically and structurally sensitive. Laser ablation and matrix isolation have been successfully employed for generation of unsaturated transition metal nitrosyl species for infrared absorption studies in our laboratory. Another challenge in infrared studies of metal nitrosyl species lies in the unambiguous identification of the nitrosyl coordination number. By carefully controlling the ablation laser power and reagent concentration, different coordinated mononuclear metal nitrosyls can be identified in infrared spectra by stepwise annealing to allow diffusion and further reaction, by mixed isotopic substitution experiments, as well as by comparison with theoretical predictions of vibrational frequencies, isotopic shifts, and relative band intensities. These experiments can also produce binuclear and trinuclear metal complexes on anneal-

ing, and such complexes can often be identified.[20] The use of isotopic mixtures and isotopic band multiplet structure in infrared spectra for determining the number of nitrosyls will be described with examples in section III.

## C. Theoretical Methods

Experience has shown that the Hartree−Fock (HF) (or self-consistent-field (SCF)) approach does not describe transition metal systems very accurately.[43] One drawback of the HF approach is the underestimation of the metal to NO electron donation; therefore, methods used to study these molecules must include electron correlation. The complete-active-space SCF (CASSCF) approach can be used to obtain some insight into the bonding, but even higher levels of theory are required for accurate results, such as the coupled-cluster singles and doubles approach, including a perturbational estimate of the triples (CCSD(T)), to obtain a more accurate description.[15,44] Although the CCSD(T) method has been used to compute bond energies and vibrational frequencies,[15] the computational cost is not practical for rapid investigations of nitrosyl species, especially those with several NO groups.

Density functional theory (DFT) is an attractive alternative to the more traditional computational approaches. The computational cost of DFT is much lower than CCSD(T), and equally importantly, analytic second derivatives make it possible to compute the harmonic frequencies of even quite large molecules at the DFT level. Calibration calculations comparing B3LYP binding energies for $MNO^+$ with the higher level CCSD(T) find the DFT values higher by 3−17 kcal/mol.[15] Experience has shown that the B3LYP[45,46] and BP86[47,48] density functionals, with moderate basis sets, and the user-friendly Gaussian 98 code[49] can provide reasonable predictions for transition metal containing compounds.[43,50] In addition, isotopic frequencies can be calculated for comparison with the observed values to determine isotopic frequency ratios as a characteristic of the normal mode and another diagnostic for identifying new species. As shown in first-row TM nitrosyl calculations, it is particularly valuable to have a systematic study.[14,15] We will follow this approach in the review that follows. Theoretical and experimental results will be compared for specific TM nitrosyl systems in section III.

# *III. Binary Transition Metal Nitrosyl Neutrals*

Binary unsaturated mononuclear transition metal nitrosyl neutrals have been investigated in the past decade using matrix infrared spectroscopy. Table 1 lists the observed N−O stretching frequencies of TM nitrosyls in solid neon and solid argon. As the more polarizable matrix interacts more strongly with host molecules, the neon matrix values are usually closer to gas-phase values and thus provide a better prediction of the yet-to-be determined gas-phase spectroscopic data. Furthermore, solid neon is more effective for trapping cations, and more information on all of the trapped species—cations, neutrals, and anions—can often be obtained from the neon matrix spectra recently obtained in our laboratory.

Unsaturated transition metal nitrosyls have been the subject of surprisingly few theoretical studies,[51] most of which are focused on mononitrosyls, and several computational methods have been used.[14,15,44] These calculations have provided accurate predictions of the equilibrium geometries, harmonic frequencies, and bonding energies. Several properties of the stable compound $Cr(NO)_4$ have been computed including geometry, absorption spectra, and electronic structure.[52−57] The latter study employed DFT to calculate structures and concluded that structural reorganizations from linear to bent metal-nitrosyls play a key role in reactions.[57] Recent DFT calculations in our laboratory provide a consistent set of vibrational frequencies for systems containing from one to three NO molecules, and therefore we will describe these calculations in the following sections.

Mixed isotopic spectra are extremely important for sorting out the coordination number, i.e., the number of NO subunits in a metal nitrosyl. In the 1/1 mixed $^{14}N^{16}O + {}^{15}N^{16}O$ isotopic experiment, Figure 2, the mononitrosyl absorption consists of a 1/1 doublet containing only the pure isotopic molecules, but the dinitrosyl exhibits one new mixed isotopic band for the $M(^{14}N^{16}O)(^{15}N^{16}O)$ isotopic molecule. For the strong antisymmetric N−O vibration not interacting with the usually weaker symmetric vibration, the $M(^{14}NO)_2$, $M(^{14}NO)(^{15}NO)$, and $M(^{15}NO)_2$ band intensities follow the statistical weights of 1/2/1. The trinitrosyl forms four isotopic molecules, and the 1/3/3/1 statistical weights for $M(^{14}NO)_3$, $M(^{14}NO)_2(^{15}NO)$,

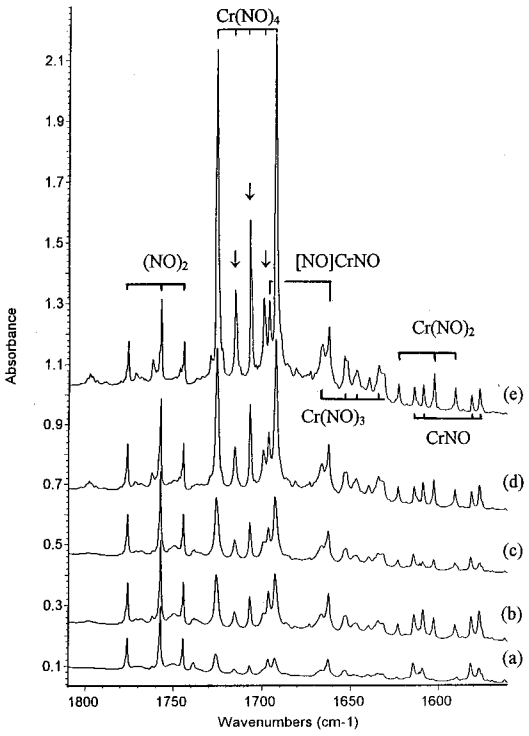


**Figure 2.** Infrared spectra in the 1810−1550 $cm^{-1}$ region for laser-ablated chromium atoms co-deposited with 0.2% $^{14}N^{16}O + 0.2\%$ $^{15}N^{16}O$ in excess argon at 10 K: (a) after 1 h deposition, (b) after 25 K annealing, (c) after 30 min broadband (240−700 nm) photolysis, (d) after annealing to 30 K, and (e) after annealing to 35 K.

**Table 1. Vibrational Stretching Frequencies ($cm^{-1}$) Observed for Neutral Binary Unsaturated Transition Metal Nitrosyls $M(NO)_n$ and $M[NO]_n$ and Insertion Products NMO in Solid Neon and Solid Argon[a]**

| | Sc[59] | Ti[59,60] | V[63,66] | Cr[26,66] | Mn[27] | Fe[24,67] | Co[25,67] | Ni[28,67] | Cu[84,85] |
|---|---|---|---|---|---|---|---|---|---|
| MNO | *1589.4* | | | *1637.3* | *1754.4* | *1766.0* | *1794.2* | *1680.1* | *1602.2* |
| | 1563.3 | | 1606.0 | 1614.3 | 1748.6 | 1748.9 | 1761.1 | 1676.6 | 1587.1 |
| | | | | 541.1 | | | 620.1 | 608.5 | 452.6 |
| | | | | | | | | | 278.2 |
| $M(NO)_2$ | *1572.9* | | *1627.8* | *1628.8* | *1705.3* | *1744.6* | *1749.1* | *1762.0* | *1637.2* |
| | | | | | *1768.9* | *1810.8* | | | *615.1* |
| | | 1531 | 1614.5 | 1623.3 | 1693.0 | 1731.6 | 1737.6 | 1749.7 | 1611.6 |
| | | | 1736.8 | | | 1798.1 | 1827.2 | 524.4 | 608.6 |
| $M(NO)_3$ | | | *1728.7* | *1675.4* | *1721.8* | *1755.7* | *1782.1* | | *1692.8* |
| | | | 1715.1 | 1663.5 | 1713.2 | 1742.6 | 1770.1 | | 1684.9 |
| | | | 1850.6 | | 1824.1 | 1798.1 | 579.3 | | |
| | | | | | 594.1 | 513.4 | 493.8 | | |
| $M(NO)_4$ | | | | *1734.5* | | | | | |
| | | | | 659.3 | | | | | |
| | | | | 1726.0 | | | | | |
| | | | | 663.0 | | | | | |
| M[NO] | *860.8* | | *1069.8* | *1123.9* | *1235.7* | *1342.2* | *1317.4* | *1292.6* | |
| | *642.6* | | 1075.7 | 1108.8 | 1236.8 | | 1284.2 | 1293.7 | |
| | 865.5 | | | 528.2 | | | | 540.5 | |
| | 644.1 | | | 478.0 | | | | 464.4 | |
| $M[NO]_2$ | | | 1153.8 | | *1270.0* | | | 1343.9 | |
| | | 1100 | 1119.6 | | 1268.7 | | | | |
| NMO | 909.5 | 900.6 | 998.1 | 976.1 | 932.3 | | | | |
| | 471.1 | 718.2 | 906.4 | 866.2 | 874.0 | | | | |

| | Y[70] | Zr[61] | Nb[65] | Mo[69] | Tc | Ru[74] | Rh[75] | Pd[79,80] | Ag[86] |
|---|---|---|---|---|---|---|---|---|---|
| MNO | *1496.2* | | | | | *1785.8* | *1806.4* | *1676.4* | *1707.3* |
| | 1484.8 | | | 1620.6 | | 1765.9 | 1775.1 | 1661.8 | 1680.3 |
| $M(NO)_2$ | | | | | | *1721.4* | *1746.9* | *1753.0* | |
| | | | | | | *1805.3* | | | |
| | | | 1583.6 | 1642.7 | | 1709.6 | 1736.5 | 1738.6 | |
| | | | | | | | 1801.8 | 433.5 | |
| $M(NO)_3$ | | | | | | *1741.1* | *1757.7* | | |
| | | | 1673.2 | 1656.4 | | 1738.9 | 1749.0 | | |
| $M(NO)_4$ | | | | 1677.5 | | | | | |
| | | | | 558.0 | | | | | |
| M[NO] | *1006.4* | | | | | | | | |
| | 1009.6 | | | | | | | | |
| NMO | | 844.2 | 977.3 | 991.1 | | 991.8 | 964.2 | | |
| | | 673.3 | 852.6 | 846.5 | | 803.0 | 813.7 | | |

| | La[70] | Hf[61] | Ta[65] | W[69] | Re[27] | Os[74] | Ir[75] | Pt[79] | Au[87] |
|---|---|---|---|---|---|---|---|---|---|
| MNO | *1416.5* | | | | | *1789.1* | *1851.1* | *1712.6* | *1710.4* |
| | 1409.0 | | | | | | 1833.7 | 1677.0 | 1701.9 |
| | | | | | | | | | 517.8 |
| $M(NO)_2$ | | | | | | *1726.9* | | *1780* | *1528.2* |
| | | | 1574.8 | 1639.2 | 1651.6 | 1717.9 | 1743.2 | 1763.9 | 1510.7 |
| | | | | | | 1815.8 | | | |
| $M(NO)_3$ | | | | | | *1753.2* | *1753.7* | | |
| | | | 1676.9 | 1655.8 | 1766.7 | 1745.5 | 1745.5 | | |
| $M(NO)_4$ | | | | 1667.4 | | | | | |
| | | | | 1664.9 | | | | | |
| M[NO] | | | | | | *1168.0* | | | |
| | | | | | 1137.0 | 1132.6 | | | |
| NMO | | 855.2 | 967.6 | 1016.3 | 1052.9 | 1052.9 | 977.3 | | |
| | | 685.3 | 855.8 | 907.3 | 901.2 | 886.9 | 850.6 | | |

[a] Neon matrix values in italics.

$M(^{14}NO)(^{15}NO)_2$, and $M(^{15}NO)_3$ apply to the symmetric nondegenerate mode. However, for the doubly degenerate mode of a trigonal complex, the mixed isotopic molecules have lower symmetry, degeneracy is lifted, and coincident band intensity addition results in a 3/1/1/3 quartet in most cases. The triply degenerate mode of the tetrahedral $Cr(NO)_4$ complex exhibits three new mixed isotopic bands often with 1/2/1 relative intensities in the center of a pentet structure.[26] Darling and Ogden describe mixed isotopic multiplet structures with varying degrees of vibrational interaction for a variety of equivalent ligands in metal carbonyls.[58]

## A. Sc Group

Infrared spectra of laser-ablated Sc and NO reaction products are particularly complicated, and their identification was greatly assisted by DFT calculations as three Sc + NO structures, ScNO, i.e., (Sc-$\eta^1$-NO), Sc[NO], i.e., (Sc-$\eta^2$-NO), and the insertion product NScO, are within 10 kcal/mol at the BP86/6-31+G*/modified Wachters-Hay level, but their vibrational spectra are very structure sensitive. Close agreement (within 20 $cm^{-1}$) between the calculated and observed argon matrix frequencies and intensities enabled all three of the above primary reaction products to be identified.[59] All of these products

increase on annealing the argon matrix to 25 K, suggesting that the reactions are spontaneous, including insertion, and require little or no activation energy. It is interesting to note that UV−vis irradiation converts side-bound Sc[NO] complex into the inserted NScO species but not to the end-bound ScNO complex. Previous DFT calculations of only the ScNO isomer also found a $^3\Pi$ ground state but predicted a nitrosyl frequency 115 $cm^{-1}$ too low, presumably owing to excessive $\pi$ back-donation.[14]

$$Sc + NO \rightarrow ScNO$$

$$Sc + NO \rightarrow Sc[NO]$$

$$Sc + NO \rightarrow NScO \qquad (2)$$

Considerable information about the nature of the vibrational mode can be obtained from the isotopic shifts or the isotopic frequency ratios. For example, $^{14}N^{16}O$ is observed in solid argon at 1871.8 $cm^{-1}$, $^{15}N^{16}O$ at 1838.9 $cm^{-1}$, and $^{15}N^{18}O$ at 1789.3 $cm^{-1}$, all ± 0.1 $cm^{-1}$. The $^{14}N^{16}O/^{15}N^{16}O = 1871.8/1838.9 = 1.01789$ and $^{15}N^{16}O/^{15}N^{18}O = 1838.9/1789.3 = 1.02772$ ratios are slightly below the calculated harmonic oscillator values (1.01820 and 1.02809) owing to a small amount of anharmonicity in the vibration of the NO molecule. (The argon matrix red shifts the vibration from 1876.1 to 1871.8 $cm^{-1}$ but has little effect on the anharmonicity.)

Thus, we compare ScNO with N−O frequency 1563.2 $cm^{-1}$ and $^{14}N^{16}O/^{15}N^{16}O = 1.01937$ and $^{15}N^{16}O/^{15}N^{18}O = 1.02438$ ratios to NO itself as reference model. Clearly there is more N and less O movement in the Sc−N−O mode than in the isolated N−O mode: this is due to motion of N between Sc and O, or in other words, coupling of the Sc−N and N−O vibrations, and it will depend on the relative position of the two frequencies (the Sc−N mode was calculated at 568.0 $cm^{-1}$ with <1% of the intensity of the N−O mode calculated at 1543.8 $cm^{-1}$) and the structure of the molecule, i.e., the Sc−N−O angle.

The triangular, side-bound Sc[NO] molecule exhibits 865.5 and 644.1 $cm^{-1}$ frequencies with $^{14}N^{16}O/^{15}N^{16}O$ ratios of 1.01418 and 1.01770, respectively, and $^{15}N^{16}O/^{15}N^{18}O$ ratios of 1.02093 and 1.02310, which show considerable mixing of Sc−N, Sc−O, and N−O motions. When the molecule opens on photolysis to give bent N−Sc−O, the frequencies are higher at 909.5 $cm^{-1}$ and lower at 471.1 $cm^{-1}$. The upper band shifts only 0.4 $cm^{-1}$ with $^{15}N^{16}O$ and gives a $^{15}N^{16}O/^{15}N^{18}O = 1.04314$ ratio; this is just below the $Sc^{16}O/Sc^{18}O$ ratio of 1.04338 and demonstrates that the 909.5 $cm^{-1}$ band is an almost pure Sc−O stretching mode. On the other hand, the lower band shifts only 0.2 $cm^{-1}$ on $^{18}O$ substitution and shows a $^{14}N^{16}O/^{15}N^{16}O = 1.02569$ ratio; this is just below the $Sc^{14}N/Sc^{15}N = 1.02619$ ratio and confirms that the 471.1 $cm^{-1}$ band is essentially a pure Sc−N stretching mode.[59]

In addition to predicting the frequencies for the ScNO, Sc[NO], and NScO isomers within 20 $cm^{-1}$, BP86 frequency calculations also accurately compute the isotopic frequencies and thus correctly describe the observed normal modes. The calculations also predict the two modes for Sc[NO] to have 2:1 relative intensity, in agreement with the observed bands, and the two absorptions for NScO to be 4:1 relative intensity, in very good agreement with the observed 3:1 ratio.

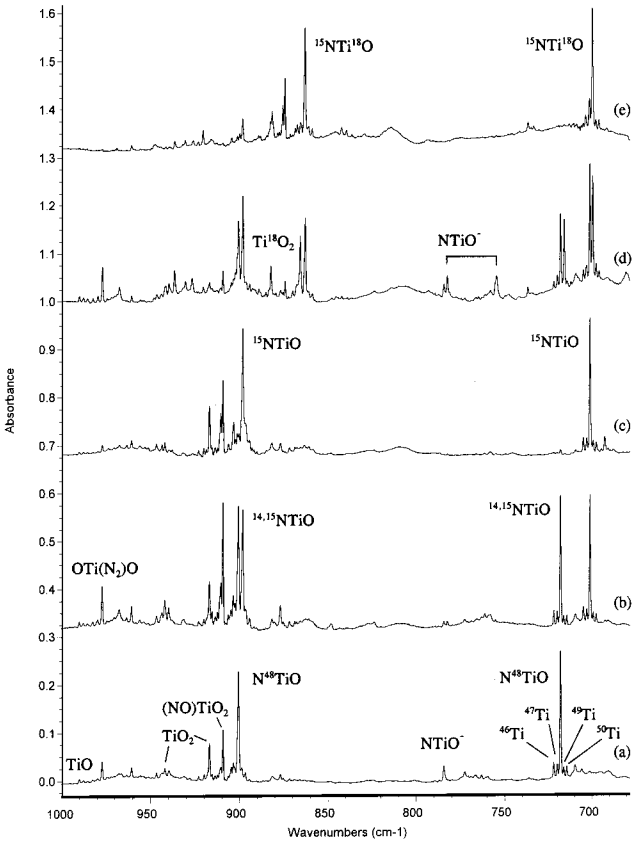


**Figure 3.** Infrared spectra of laser-ablated Ti atoms codeposited with isotopic NO reagents in argon at 7−8 K recorded after annealing to 34 ± 2 K: (a) 0.2% $^{14}N^{16}O$, (b) 0.15% $^{14}N^{16}O$ and 0.15% $^{15}N^{16}O$, (c) 0.2% $^{15}N^{16}O$, (d) 0.06% $^{15}N^{16}O$ and $^{15}N^{18}O$ and 0.04% $^{14}N^{16}O$ and $^{14}N^{18}O$, and (e) 0.2% $^{15}N^{18}O$.

Accordingly, the frequency calculations provide not only predictions of fundamental frequencies for new molecules but isotopic frequencies to describe structure sensitive normal modes and relative intensities to further characterize these modes.

## B. Ti Group

Titanium atom reactions with NO have been investigated in the Charlottesville and Paris matrix-isolation laboratories.[59,60] The products are dominated by strong, sharp 900.6 and 718.2 $cm^{-1}$ absorptions that show natural titanium isotopic splittings with relative intensities in agreement with natural abundance Ti, which indicates that a single Ti atom is involved in these vibrational modes (Figure 3). Investigations with $^{14}N^{16}O/^{15}N^{16}O$ and $^{15}N^{16}O/^{15}N^{18}O$ mixtures revealed only pure isotopic bands, which shows that single N and O atoms contribute to these vibrational modes. Further information about the vibrational modes comes from the magnitudes of the isotopic shifts for each band. The $^{14}N^{48}Ti^{16}O$ bands at 900.6 and 718.2 $cm^{-1}$ shift to 898.2 and 701.2 $cm^{-1}$ for $^{15}N^{48}Ti^{16}O$ and to 862.9 and 699.7 $cm^{-1}$ for $^{15}N^{48}Ti^{18}O$. These shifts demonstrate that the upper

band is primarily a Ti−O, and the lower band essentially a Ti−N stretching mode. A pure Ti-$^{16}$O oscillator at 898.2 cm$^{-1}$ would shift to 861.4 cm$^{-1}$ for Ti-$^{18}$O and a pure Ti-$^{14}$N vibrator at 718.2 cm$^{-1}$ would shift to 699.6 cm$^{-1}$ for Ti-$^{15}$N. Accordingly, this new molecule was identified as the NTiO insertion product.

The most amazing observation is that the NTiO bands *increase* by a factor of 5 on annealing the 7 K argon matrix to 25 K. In fact, both bands increase by 20% on first annealing to 14 K; hence, it was assumed that 14 K represents the onset of diffusion of Ti and/or NO in solid argon and that, at 14 K, the Ti + NO insertion reaction is spontaneous.[59] Apparently the insertion reaction 3 requires virtually no activation energy. The ground state Ti + NO reaction has recently been investigated by gas-phase crossed beams, and the kinetic energy threshold for the exothermic (−36 kJ/mol) abstraction reaction to form TiO is 2 ± 1 kJ/mol.[61] The BP86 calculations accurately predict the NTiO isotopic frequencies (within 1.7, 0.5, 0.3, and 2.6 cm$^{-1}$) and the relative band intensities (within 10%). Furthermore, the calculations predict the side-bound Ti[NO] $^2$A′ complex 20.8 kcal/mol higher and the end-bound $^2\Sigma^+$ TiNO complex 36.5 kcal/mol higher than the lowest $^2$A′ NTiO isomer.[59] Accordingly, it appears unlikely that the higher energy isomers can be trapped in the matrix.

$$\mathrm{Ti} + \mathrm{NO} \xrightarrow[\text{solid argon}]{14\mathrm{K}} \mathrm{NTiO}\ (^2\mathrm{A}') \qquad (3)$$

A recent thermal Ti atom and NO investigation found the same NTiO spectrum as the laser-ablation work, confirmed reaction 3, and with a higher product yield, observed the bending mode at 248.2 cm$^{-1}$ and overtones at 1430.7 and 1791.5 cm$^{-1}$. The Paris group also found a higher order dependence for the 1614.7 cm$^{-1}$ band first attributed to TiNO and showed this assignment to be incorrect.[60] These workers observed 1531 and 1100 cm$^{-1}$ bands for Ti(NO)$_2$ and Ti[NO]$_2$, which arise from the Ti + (NO)$_2$ reaction. Kushto et al. identified the two most stable such products as OTi(N$_2$)O and (NN)TiO$_2$.[59]

Subsequent work has shown that laser-ablated Zr and Hf atoms also react with NO to form bent NMO insertion products.[62] These favorable reactions proceed on annealing to 21−24 K, and the NMO molecules are characterized by isotopic substitution and M−O stretching modes at 844.2 and 855.2 cm$^{-1}$ and M−N stretching modes at 673.3 and 685.3 cm$^{-1}$, respectively. The increase in bond stretching frequencies from Zr to Hf is probably due to the larger relativistic bond-length contraction and resulting force-constant increase for Hf to Th.[63] The BP86 functional and averaged relativistic effective potentials for Zr and Hf predict bent $^2$A′ states and observed frequencies within 1−3% and the isotopic shifts within 2 cm$^{-1}$.

## C. V Group

Laser-ablated vanadium atoms have been reacted with NO molecules during condensation in excess argon.[64] Absorptions due to NVO (998.1, 906.4 cm$^{-1}$), V-$\eta^1$-NO (1606.0 cm$^{-1}$), and V-$\eta^2$-NO (1075.7 cm$^{-1}$) structural isomers were observed and identified via isotopic substitution and DFT calculations. Higher nitrosyls were also formed on annealing. On the basis of the observed isotopic multiplet patterns, bands at 1614.5 and 1736.8 cm$^{-1}$ were assigned to antisymmetric and symmetric N−O vibrations of the $C_{2v}$ dinitrosyl V(NO)$_2$, and 1715.1 and 1850.6 cm$^{-1}$ bands were assigned to the analogous vibrations of V(NO)$_3$ with $C_{3v}$ symmetry.

Recent DFT calculations find NVO ($^1$A′) to be the lowest energy isomer, and the initial deposited spectrum is dominated by strong NVO absorptions.[64] However, on annealing, weak VNO and V[NO] bands increase markedly while NVO absorptions double. These bands show mixed isotopic doublets for the participation of a single NO molecule. The BP86 calculations predicted VNO ($^3\Delta$) to be 41.0 kcal/mol and V[NO] ($^3$A″) to be 45.4 kcal/mol higher than NVO. Although Blanchet et al. did not calculate NVO and V[NO], these workers find a $^3\Delta$ ground state for VNO and 1608 cm$^{-1}$ frequency using DFT,[14] which is comparable to the 1627 cm$^{-1}$ BP86 calculated and 1606 cm$^{-1}$ argon matrix values. It is perhaps surprising that the higher energy VNO and V[NO] isomers can be formed and stabilized in the cold matrix: this requires barriers on the potential energy surface between VNO, V[NO], and the more stable NVO that are easily surmounted during the deposition process but not on annealing solid argon to 25 K. In contrast the barriers between TiNO, Ti[NO], and NTiO are much smaller, and only the more stable NTiO isomer is trapped following the cold reaction of Ti and NO on annealing.

On further annealing to 30 and 35 K, the higher V(NO)$_2$ and V(NO)$_3$ nitrosyls became dominant. Mixed isotopic spectra show splittings for two and three equivalent NO subunits in these molecules. Recent BP86 calculations predict a bent $^2$A′ ground state for V(NO)$_2$ and a pyramidal $^3$A″ ground state for V(NO)$_3$ with frequencies and isotopic frequency ratios in very good agreement.[64] The optimized structure for the trinitrosyl is very close to $C_{3v}$ but slightly distorted to $C_s$ symmetry (∠VNO: 170.8, 171.1°; VN: 1.7665, 1.7660 Å). It is interesting to compare the $^{14}$N$^{16}$O/$^{15}$N$^{16}$O and $^{15}$N$^{16}$O/$^{15}$N$^{18}$O isotopic ratios for the N−O stretching modes of VNO, V(NO)$_2$, and V(NO)$_3$. For VNO, the ratios 1.02023 and 1.02307 indicate substantial V−N, N−O coupling; this coupling diminishes for V(NO)$_2$ where the respective ratios are 1.01834 and 1.02625 for the antisymmetric and 1.01967 and 1.02429 for the symmetric N−O stretching mode, but note more coupling in the symmetric than the antisymmetric mode for the dinitrosyl. The coupling diminishes still further for the trinitrosyl with 1.01819 and 1.02566 ratios for the very strong antisymmetric and 1.01940 and 1.02479 for the weak symmetric mode as the pure diatomic NO ratios are approached. The isotopic frequency ratios as a description of the normal mode are accurately modeled by the DFT frequency calculations.[64]

Laser-ablated Nb and Ta atoms react with NO to give primarily the NNbO and NTaO insertion products, which were identified from isotopic substitution

and density functional calculations of isotopic frequencies.[65] Although the mononitrosyls were not observed, annealing produced dinitrosyls and trinitrosyls for both metals. Photolysis markedly increased $(N_2)(NbO_2)$ and $(N_2)(TaO_2)$, which are the most stable end products for the metal atom reactions with $(NO)_2$.

## D. Cr Group

Laser-ablated chromium atoms were reacted with NO molecules during condensation in excess argon.[26] Absorptions due to NCrO (976.1, 866.2 $cm^{-1}$), Cr-$\eta^1$-NO (1614.3, 541.1 $cm^{-1}$), and Cr-$\eta^2$-NO (1108.8, 528.2, 478.0 $cm^{-1}$) were observed after sample deposition and identified via isotopic substitution and DFT frequency calculations. The insertion reaction to give the more stable NCrO product required activation energy, while the addition products Cr-$\eta^1$-NO and Cr-$\eta^2$-NO were formed on diffusion of the cold reagents in solid argon. Higher nitrosyls were also produced on annealing as will be discussed in detail here.

**CrNO Also Cr-$\eta^1$-NO.** Sharp 1614.3 and 1609.1 $cm^{-1}$ bands observed after deposition increased markedly on first annealing to 25 K, slightly increased on 30 and 35 K annealing, but slightly decreased on further annealing to 40 K as illustrated in Figure 4A. In the low NO concentration experiments, the yield of these bands increased relative to the 1623.3, 1663.5, and 1726.0 $cm^{-1}$ higher nitrosyl bands. Two weaker bands at 541.1 and 533.3 $cm^{-1}$ behaved the same as the 1614.3 and 1609.1 $cm^{-1}$ bands; these absorptions are due to the same product in different local matrix site environments. The isotopic 14−16/15−16 ratios for the upper two bands are 1.02087 and 1.02061, slightly higher than the diatomic NO ratio (1.01789), while the 15−16/15−18 ratio 1.02257 is lower than the diatomic NO ratio (1.02778), which means that the N atom is moving between O and another atom. Furthermore, the mixed isotopic doublet (Figure 2) verifies the vibration of a single NO subunit.

The CrNO assignment is supported by DFT calculations. Blanchet et al.[14] calculated the N−O and Cr−NO stretching frequencies for the $^4\Sigma^-$ ground state to be 1607 and 595 $cm^{-1}$. The computed N−O stretching mode is very close to the experimental observation, while the Cr−NO mode is slightly higher than the observed value. Our BP86/6-311+G*/modified Wachters−Hay calculation predicted 1653.9 and 601.0 $cm^{-1}$ for these two modes, which are 2.4 and 11.1% too high; however, the calculated isotopic ratios and intensities are in excellent agreement with the experimental values.[26] Note that the N−O stretching mode is calculated more accurately than the Cr−N stretching mode. The calculated 14−16/15−16 and 15−16/15−18 isotopic ratios for the upper mode are 1.02137 and 1.02229, very close to the observed 1.02087 and 1.02257 ratios, while for the lower mode, calculations give 1.0072 and 1.02543, and experiments provide 1.0070 and 1.02437 ratios, respectively.

The CrNO absorptions markedly increased on first annealing and slightly decreased on later annealing, indicating that CrNO can be formed on diffusion of cold reagents in solid argon and can react further with NO to form higher nitrosyls:

$$Cr + NO \rightarrow CrNO \quad (4)$$

$$CrNO + NO \rightarrow Cr(NO)_2 \quad (5)$$

$$Cr(NO)_2 + NO \rightarrow Cr(NO)_3 \quad (6)$$

$$Cr(NO)_3 + NO \rightarrow Cr(NO)_4 \quad (7)$$

The decrease of NO and increase of $(NO)_2$ absorptions on annealing attests to the diffusion and reaction of NO under these conditions.

**$Cr(NO)_2$ Also Cr-($\eta^1$-NO)$_2$.** The next band that increases on annealing in the nitrosyl region is at 1623.3 $cm^{-1}$, and the intensity relative to CrNO is greater in higher concentration NO experiments. This band shifts to 1590.7 $cm^{-1}$ in the $^{15}N^{16}O$ experiment and to 1555.5 $cm^{-1}$ with $^{15}N^{18}O$, which exhibits 1.02049 and 1.02263 isotopic 14−16/15−16 and 15−16/15−18 ratios that are very similar to the ratios for CrNO. The 1:2:1 triplet observed for both 14−16/15−16 (Figure 2) and 15−16/15−18 isotopic mixtures indicates that two equivalent NO submolecules are involved in this vibration. Clearly the 1623.3 $cm^{-1}$ band is appropriate for the $Cr(NO)_2$ molecule.[26]

Similar DFT calculations found a bent $^3B_2$ $Cr(NO)_2$ molecule with a very strong antisymmetric N−O stretching fundamental at 1656.8 $cm^{-1}$, just 3 $cm^{-1}$ above CrNO, which is in good agreement with experiment.[26] The calculated isotopic ratios, 1.02051 and 1.02384, are very close to the observed ratios. The symmetric N−O stretching mode, calculated to be much weaker, was not observed.

**$Cr(NO)_3$ Also Cr-($\eta^1$-NO)$_3$.** The 1663.5 and 1668.7 $cm^{-1}$ bands observed on deposition doubled on first annealing to 25 K, increased slightly on subsequent annealing to 30, 35, and 40 K, while the 1726.0 $cm^{-1}$ band due to $Cr(NO)_4$ greatly increased (Figure 4A). In lower concentration NO experiments, similar behavior was observed, but the growth on annealing was less pronounced. The isotopic ratios (14−16/15−16: 1.01955 and 15−16/15−18: 1.02436) are characteristic nitrosyl ratios. In both 14−16/15−16 (Figure 2) and 15−16/15−18 mixed isotopic experiments, quartets with approximately 2:2:1:2 relative intensities were observed, suggesting that three NO molecules are involved in an antisymmetric stretching mode, and the $Cr(NO)_3$ molecule is identified.[26]

Very recent DFT calculations converged a $^2A'$ pyramidal $Cr(NO)_3$ complex in $C_s$ symmetry with two equivalent Cr−N−O linkages (1.720, 1.185 Å) and a third with slightly different (1.714, 1.180 Å) bond distance.[66] Accordingly, the two strongest N−O stretching modes were slightly different, 1695.6 and 1707.5 $cm^{-1}$, but in the chromium nitrosyl trend, and two bands are observed in the matrix spectrum at 1663.5 and 1668.7 $cm^{-1}$. Furthermore, the mixed isotopic multiplet pattern is not of the relative intensities usually associated with a doubly degenerate mode.[58]

**$Cr(NO)_4$ Also Cr-($\eta^1$-NO)$_4$.** Chromium tetranitrosyl, $Cr(NO)_4$, is a stable 18-electron system, and

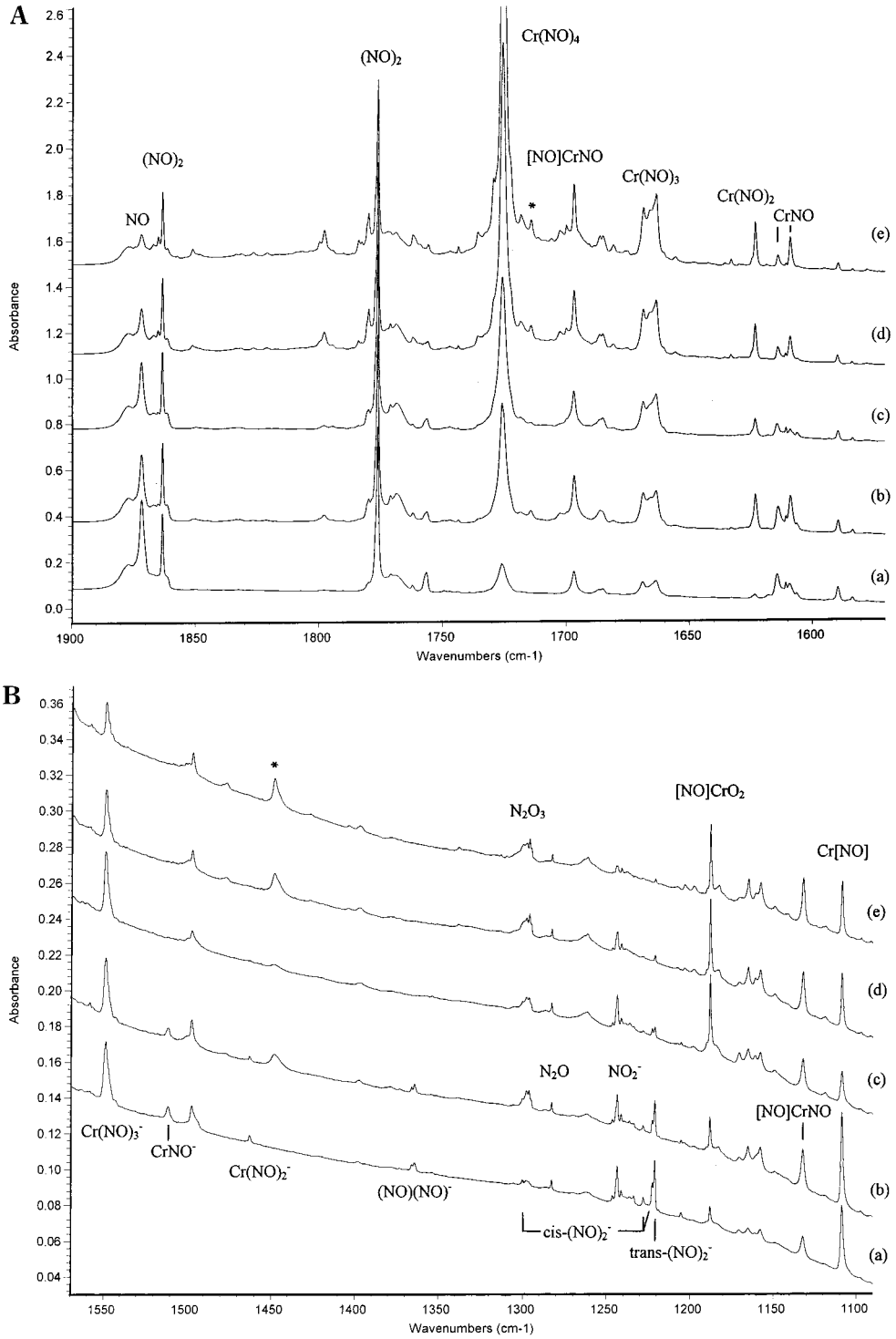


**Figure 4.** (A) Infrared spectra in the 1900−1570 $cm^{-1}$ region for laser-ablated chromium atoms co-deposited with 0.4% NO in argon on a 10 K CsI window: (a) after 1 h sample co-deposition at 10 K, (b) after annealing to 25 K, (c) after broadband (240−700 nm) photolysis for 30 min, (d) after annealing to 30 K, and (e) after annealing to 35 K. Key: * = $Cr(NO)_3(NO)$*. (B) Infrared spectra in the 1570−1090 $cm^{-1}$ region for laser-ablated chromium atoms co-deposited with 0.4% NO in argon on a 10 K CsI window: (a) after 1 h sample co-deposition at 10 K, (b) after annealing to 25 K, (c) after broadband photolysis for 30 min, (d) after annealing to 30 K, and (e) after annealing to 35 K. Key: * = $Cr(NO)_3(NO)$*.

the only pure transition metal nitrosyl that has been isolated and characterized.[36] A strong NO stretching mode at 1725.5 $cm^{-1}$ and a deformation band at 662.1 $cm^{-1}$ have been observed in an argon matrix deposit containing the authentic material.[29] In Cr + NO experiments, the 1726.0 $cm^{-1}$ band observed after deposition at higher NO concentrations greatly increased on annealing and became the strongest band in the experiments. Isotopic ratios again denote a nitrosyl vibration. Both mixed isotopic 14−16/15−16 and 15−16/15−18 experiments revealed a strong mixed isotopic pentet characteristic of a triply degenerate mode,[58] and the assignment to tetrahedral $Cr(NO)_4$ is confirmed.[26] Two weaker bands at 663.0 and 506.1 $cm^{-1}$ track with the 1726.0 $cm^{-1}$ band. The 663.0 $cm^{-1}$ band has a very low 14/15 isotopic ratio

(1.01113), while the 506.1 $cm^{-1}$ band has a high 14/15 ratio (1.02221). These two bands are due to mixed triply degenerate Cr−N−O deformation and Cr−NO stretching modes of the $Cr(NO)_4$ molecule.

Calculations for $Cr(NO)_4$ gave a $^1T_2$ ground state tetrahedral structure with 1.743 and 1.174 Å Cr−N and N−O bond lengths and $t_2$ fundamentals at 1753.0, 705.2, and 526.1 $cm^{-1}$, which are slightly higher than the observed frequencies, as expected.[26,66] The calculated isotopic frequency ratios are in excellent agreement with the observed ratios including the lower frequency modes involving Cr−N−O deformation and Cr−NO stretching. The scale factors (observed/calculated frequencies) for $Cr(NO)_{1-4}$ are 0.976, 0.980, 0.981−0.977, and 0.985, respectively, which are appropriate for the BP86 functional.[43]

Irradiation of $Cr(NO)_4$ in solid argon gave rise to two sets of bands at 1714, 1711 and 1703, 1699 $cm^{-1}$ and at 1450 $cm^{-1}$, which were ascribed to a species with a nitrosyl ligand in a different mode of coordination.[29] Laser-ablation experiments produced the latter feature at 1448.8 $cm^{-1}$ on annealing (Figure 4B) and demonstrated a small secondary isotopic effect: the $^{14}N^{16}O$ + $^{15}N^{16}O$ experiment gave a 1448.4−1423.4 $cm^{-1}$ doublet with the pure $^{15}N^{16}O$ band at 1423.0 $cm^{-1}$, which means that a single NO subunit is slightly coupled to other NO groups. The $^{14}N^{16}O/^{15}N^{16}O$ and $^{15}N^{16}O/^{15}N^{18}O$ isotopic ratios, 1.01811 and 1.02644, reveal a small amount of mode mixing, much less than for linear CrNO. This 1448.8 $cm^{-1}$ absorption is intermediate between linear CrNO (1614.3 $cm^{-1}$) and side-bound Cr[NO] (1108.8 $cm^{-1}$), which suggests either a bent Cr−N−O bond or more likely the effect of less electron density available on the Cr center in a higher nitrosyl like $Cr(NO)_3[NO]$ where the unique nitrosyl is probably side-bonded.

The laser-ablation experiments[26] also revealed a stronger absorption at 1714.2 $cm^{-1}$ that tracks with the 1448.8 $cm^{-1}$ band on annealing and decreases on UV irradiation, as reported previously,[29] and shifts to 1681.7 $cm^{-1}$ with $^{15}N^{16}O$ and to 1640.7 $cm^{-1}$ with $^{15}N^{18}O$. These isotopic ratios, 1.01933 and 1.02499, are comparable to those for normal nitrosyls. The position of the 1714.2 $cm^{-1}$ band between the antisymmetric N−O modes for $Cr(NO)_{3,4}$ is in accord with this being such a mode for the $Cr(NO)_3$ subunit in the $Cr(NO)_3[NO]$ complex.[29]

Similar DFT calculations were performed for a Cr-($\eta^1$-NO)$_3$-($\eta^2$-NO) complex, but this structure ultimately converged to the $T_d$ $Cr(NO)_4$ molecule. A like calculation for Cr-($\eta^1$-NO)$_2$($\eta^2$-NO) converged to Cr-($NO_3$). Although we were not able to find a stable minimum for $Cr(NO)_3[NO]$, we believe that this species is formed in the matrix experiments.[26,29] Evidence has also been found for the Cr(NO)[NO] species in these experiments[26] and calculations.[66]

**Cr[NO] Also Cr-$\eta^2$-NO.** The 1108.8 $cm^{-1}$ absorption observed after deposition increased on annealing but almost disappeared on photolysis. In $^{15}N^{16}O$ experiments this band shifts to 1090.2 $cm^{-1}$, and in $^{15}N^{18}O$ experiments to 1062.6 $cm^{-1}$. Both isotopic ratios, 1.01706 and 1.02597, are slightly lower than the diatomic NO ratio but still indicate an N−O stretching mode. A doublet is observed in the mixed 14−16/15−16 and 15−16/15−18 experiments, so another CrNO isomer is formed. Note that two very weak bands at 528.2 and 478.0 $cm^{-1}$ go with the 1108.8 $cm^{-1}$ absorption. The 528.2 $cm^{-1}$ band exhibits a high $^{14}N^{16}O/^{15}N^{16}O$ ratio (1.02444) and a low $^{15}N^{16}O/^{15}N^{18}O$ ratio (1.00233) while the 478.0 $cm^{-1}$ band has low $^{14}N^{16}O/^{15}N^{16}O$ ratio (1.00400) and high $^{15}N^{16}O/^{15}N^{18}O$ ratio (1.0397). The calculated ground state for cyclic Cr[NO] is also a quartet, only 10.8 kcal/mol higher in energy than the CrNO molecule.[26] Note that the calculated 1101.6 $cm^{-1}$ frequency for the N−O stretching mode is very close to the observed 1108.8 $cm^{-1}$ value. The calculated isotopic ratios for three modes of Cr[NO] are in excellent agreement with the experimental values, and these three bands are assigned to the cyclic or sideways bonded Cr[NO] molecule.[26]

The Cr[NO] absorptions observed after deposition increased on first annealing, so this molecule can be formed from cold reagents without activitation energy. The CrNO and Cr[NO] absorptions decreased on irradiation, suggesting photochemical rearrangement to the more stable NCrO isomer. Recent BP86 calculations find $^2A''$ NCrO to be the most stable isomer with $^4\Sigma^-$ CrNO 5.6 kcal/mol higher and $^4A''$ Cr[NO] 16.4 kcal/mol higher.[26] It is noteworthy that NCrO *does not* increase on annealing in these experiments, suggesting activation energy for the insertion reaction and substantial barriers separating the CrNO and Cr[NO] species from the slightly more stable NCrO insertion product. Finally, absorptions have been observed at 1696.8 and 1132.2 $cm^{-1}$ for [NO]CrNO with both end- and side-bound nitrosyl groups.[26]

$$Cr + NO \rightarrow Cr[NO] \quad (8)$$

$$CrNO \text{ and } Cr[NO] \xrightarrow{UV} NCrO \quad (9)$$

The $Cr(NO)_{1-4}$ absorptions have been observed in solid neon, blue shifted 23.0, 5.5, 11.9, and 8.5 $cm^{-1}$, respectively, and Cr[NO] was blue shifted 15.1 $cm^{-1}$.[66] These are typical of TM nitrosyls for the different matrix interactions.[67,68] However, Cr[NO] was trapped less effectively relative to NCrO in solid neon than in solid argon.

**Mo and W Reactions.** Laser-ablated Mo and W atoms reacted with NO to give primarily the insertion products NMoO and NWO, but weak MoN and WN absorptions are also observed.[69] The NMoO and NWO molecules were identified from isotopic substitution ($^n$Mo, $^{15}N$, $^{18}O$) and DFT calculations. The M−N and M−O stretching frequencies of the $^2A'$ state NMoO and NWO molecules were predicted by DFT (scale factors 0.936 ± 0.004 and 0.966 ± 0.005, respectively), but more importantly, the isotopic shifts (and normal modes) were well-described by DFT isotopic frequencies. The higher energy MoNO isomer was observed, but WNO and the M-$\eta^2$-NO complexes were not found. The M-($\eta^1$-NO)$_x$ ($x$ = 2,3,4) complexes are observed: mixed isotopic splittings indicate that Mo-$(NO)_4$ is tetrahedral, like $Cr(NO)_4$, but the spectra show that $W(NO)_4$ is distorted to $C_{2v}$ symmetry.

## E. Mn Group

Reactions of thermal and laser-ablated Mn atoms with NO produced the Mn-($\eta^1$-NO)$_x$ complexes ($x$ = 1−3) and a series of ($\eta^2$-NO) complexes, and in addition, laser-ablated Mn formed the NMnO insertion product.[27] The $C_{2v}$ complex Mn(NO)$_2$ in the $^2A_1$ ground state was identified from symmetric ($a_1$) and antisymmetric ($b_2$) N−O ligand stretching modes, which gave triplet mixed isotopic spectra and excellent agreement with DFT calculations. The Mn(NO)$_3$ complex was shown to have $C_{3v}$ symmetry from mixed isotopic spectra for four vibrational modes, including the symmetric ($a_1$) and antisymmetric (e) N−O ligand stretching modes, and a match with DFT calculations of isotopic frequencies. Recent BP86 calculations located three low-energy isomers: the insertion product NMnO ($^3A''$) is the global minimum, $^5A''$ and $^3\Sigma^-$ MnNO are +4.2 and +7.1 kcal/mol, and $^3A''$ Mn[NO] is +19.8 kcal/mol.[27] Blanchet et al. considered only the MnNO arrangement and found the same energy ordering of states with the bent pentet ground state.[14]

The NMnO insertion product is formed on deposition with laser-ablated Mn atoms and on sample irradiation, but not on annealing without irradiation, nor with thermal Mn atoms.[27] However, annealing increases Mn[NO], Mn[MO]$_2$, a weak band tentatively assigned to MnNO, and Mn(NO)$_{2,3}$ absorptions as these latter products also form with thermal Mn atoms. The MnNO band at 1748.6 cm$^{-1}$ is in very good agreement with DFT predictions for the triplet and not the pentet state, which suggests the triplet ground state for MnNO.[27] The Mn(NO)$_{2,3}$ molecules were identified from mixed isotopic spectra and DFT frequency calculations. It is relevant that ultraviolet irradiation of Mn(NO)$_3$(CO) in solid argon produced two sets of new absorptions: one set was assigned to a modified precursor form Mn(CO)(NO)$_2$(NO)* characterized by a new band at 1500 cm$^{-1}$, and the latter set at 1714, 1710 cm$^{-1}$ was assigned to Mn(NO)$_3$.[30] The latter set is in agreement with the strong 1713.2 cm$^{-1}$ antisymmetric fundamental for Mn(NO)$_3$ described above, and the former set with bands produced by the Mn, CO, and NO reaction, which gave the band characteristic of a different bonding mode at 1504.6 cm$^{-1}$ with $^{14}N^{16}O/^{15}N^{16}O$ and $^{15}N^{16}O/^{15}N^{18}O$ isotopic ratios 1.01814 and 1.02689 that indicate little coupling to other vibrations.[33] The recent observation of Mn(CO)(NO)$_2$(NO)* from the reagent molecules and DFT calculations support the earlier characterization of this NO complex with a different bonding mode,[30,33] which we believe to be sideways ($\eta^2$) bonded. The band appearing at 1487 cm$^{-1}$ on annealing in Mn/NO experiments is probably due to a similar Mn(NO)$_x$[NO] species.[27] These matrix-isolation observations underscore the importance of side-bound nitrosyls, which are relevant to very recent work on metastable TM-nitrosyl isomerization processes.[6,7]

Laser-ablated Re atoms gave the analogous major products, which are dominated by NReO,[27] as expected from the Cr group observations.

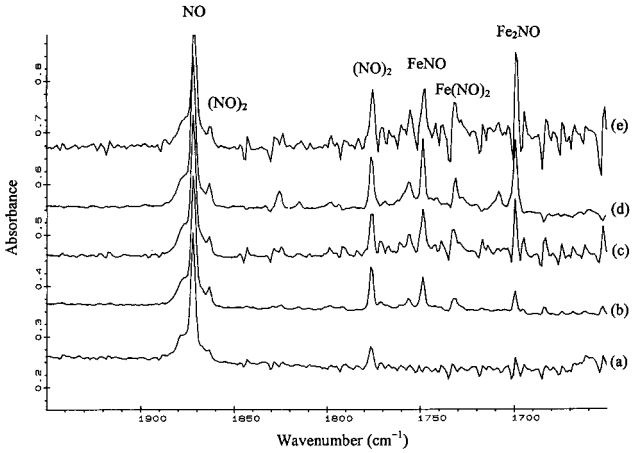


**Figure 5.** Infrared spectra in the 1940−1650 cm$^{-1}$ region for thermal iron atoms co-deposited with NO in excess argon at 12−14 K: (a) 0.5% NO in argon only, (b) 0.5% NO in argon with Fe, and (c), (d), and (e) follow with increased Fe concentration. (Figure relabeled from ref 24; reprinted with permission. Copyright 1995 Elsevier.)

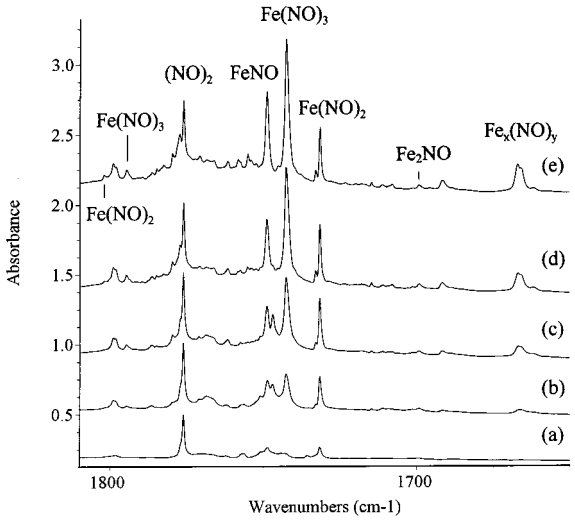


**Figure 6.** Infrared spectra in the 1810−1650 cm$^{-1}$ region from co-deposition of laser-ablated iron with 0.3% NO in argon: (a) after 1 h sample deposition at 10 K, (b) after annealing to 25 K, (c) after annealing to 30 K, (d) after annealing to 35 K, and (e) after annealing to 40 K.

## F. Fe Group

Thermal and laser-ablated iron atoms react with NO to give FeNO and Fe(NO)$_2$ at 1748.9 and 1731.6 cm$^{-1}$ on sample condensation,[24,67] and representative spectra are compared for each method in Figures 5 and 6. Annealing in the latter experiments produced new 1798.1 and 1742.6 cm$^{-1}$ absorptions for Fe(NO)$_3$, a weak new 1699.2 cm$^{-1}$ band with 1691.6 cm$^{-1}$ satellite for Fe$_2$NO, and a stronger new absorption at 1667.0 cm$^{-1}$ for the higher Fe$_x$(NO)$_y$ complex.[70] Increasing the Fe concentration with the former method favored the Fe$_2$NO band relative to the FeNO absorption at constant NO concentration. The weak 1699.2 cm$^{-1}$ band gave a $^{15}N^{16}O$ shift to 1665.2 cm$^{-1}$ and a $^{15}N^{18}O$ displacement to 1627.9 cm$^{-1}$ and showed no intermediate components in mixed isotopic samples so its first identification as Fe$_2$NO is substantiated. The $^{14}N^{16}O/^{15}N^{16}O$ and $^{15}N^{16}O/^{15}N^{18}O$ isotopic ratios for Fe$_2$NO, 1.0204 and 1.0229, are near

the FeNO values and show comparable Fe−N, N−O mode coupling. The NO frequency is reduced more on bonding to $Fe_2$ than to Fe atom. Finally, we note that ground state Fe atoms react with NO in argon buffer gas 2 orders of magnitude faster than with CO.[71] In a recent matrix-isolation investigation with both NO and CO present, FeNO products were favored.[34]

The 1748.9 $cm^{-1}$ FeNO band was the strongest after deposition in lower NO concentration experiments, and it increased on lower temperature annealing. In the mixed $^{14}N^{16}O + {}^{15}N^{16}O$ and $^{15}N^{16}O + {}^{15}N^{18}O$ experiments, only pure isotopic counterparts were present, which confirms the involvement of only one NO subunit and the FeNO assignment.[67] The weak 1731.6 $cm^{-1}$ band after sample deposition increased markedly on lower temperature annealing. In the mixed $^{14}N^{16}O + {}^{15}N^{16}O$ and $^{15}N^{16}O + {}^{15}N^{18}O$ experiments, triplets with approximately 1:2:1 relative intensities were produced, which indicate that two equivalent NO submolecules are involved. This band is assigned to the antisymmetric N−O stretching vibration of the $Fe(NO)_2$ molecule; a weak band at 1798.1 $cm^{-1}$ tracked with the 1731.6 $cm^{-1}$ band, also exhibited nitrosyl N−O stretching vibrational frequency ratios, and is assigned to the symmetric N−O stretching vibration. A much weaker band at 3503.3 $cm^{-1}$ (1% of 1731.6 $cm^{-1}$) is due to the combination band, which is 26.4 $cm^{-1}$ below the sum of stretching fundamentals and supports their assignment.[67]

The 1742.6 $cm^{-1}$ band appeared on annealing and became the strongest band after higher temperature annealing. In the mixed $^{14}N^{16}O + {}^{15}N^{16}O$ experiment, a quartet band with approximately 3:1:1:3 relative intensities is characteristic of the doubly degenerate mode of a trigonal species.[58,67] Accordingly, the 1742.6 $cm^{-1}$ band was assigned to the antisymmetric N−O stretching vibration of the $Fe(NO)_3$ molecule. A weak associated band at 1794.6 $cm^{-1}$ showed a slightly higher 14/15 ratio and a quartet with approximately 1:3:3:1 relative intensities, which is characteristic of the nondegenerate vibration mode of a trigonal species; hence, this band was assigned to the symmetric N−O stretching vibration of the $Fe(NO)_3$ molecule with $C_{3v}$ symmetry.[67] A weak band at 513.4 $cm^{-1}$ exhibited the same annealing and photolysis behavior as the 1742.6 $cm^{-1}$ band and gave a large 14/15 ratio (1.0270) and small 16/18 ratio (1.0085). In the mixed $^{14}N^{16}O + {}^{15}N^{16}O$ experiment, a quartet was also observed. This band is due to the antisymmetric Fe−NO stretching vibration of the $Fe(NO)_3$ molecule. The antisymmetric N−O stretching vibrations of $Fe(NO)_2$ and $Fe(NO)_3$ were observed at 1744.6 and 1757.8 $cm^{-1}$ in solid neon, which are blue-shifted 13.0 and 15.2 $cm^{-1}$ from argon matrix band positions. The FeNO vibration was observed at 1766.0 $cm^{-1}$ in solid neon, a straightforward 17.1 $cm^{-1}$ blue shift, and at 1746.8 $cm^{-1}$ in solid nitrogen, a small 2.1 $cm^{-1}$ red shift.[67,72]

The assignments are strongly supported by DFT calculations. Previous calculations reported a $^2\Delta$ ground state for FeNO;[14,24] recent DFT calculations predicted 1785.7 $cm^{-1}$ (BP86) and 1775.7 $cm^{-1}$ (B3LYP) N−O stretching frequencies for $^2\Delta$ ground state FeNO, which are in good agreement with the observed value.[67] Note that Blanchet et al. found a quartet state 1.9 kcal/mol higher with a 1629 $cm^{-1}$ frequency; this frequency is not compatible with the observed ground state, which shows, at least in the FeNO case, that the DFT calculations have the correct order of states in the argon and neon matrix environments. It is unlikely that the gas-phase ground state will be different from the solid neon matrix. The BP86 calculation predicted a bent $^1A_1$ ground state for $Fe(NO)_2$ with antisymmetric and symmetric N−O stretching vibrations at 1752.4 and 1825.6 $cm^{-1}$. The $Fe(NO)_3$ molecule was calculated to have a $^2A_1$ ground state with $C_{3v}$ symmetry; the antisymmetric and symmetric N−O and antisymmetric Fe−NO stretching vibrations were predicted at 1775.0, 1861.9, and 537.5 $cm^{-1}$, in excellent agreement with observed values.[67] Thus, with ∠FeNO = 170°, $Fe(NO)_3$ is a 17-electron molecule.

New 1343.8 and 1342.5 $cm^{-1}$ absorptions characterize the Fe-($\eta^2$-NO) complex in solid argon and neon based on doublet isotopic structure in the mixed isotopic experiments. A 1342.5 $cm^{-1}$ site increased on annealing in argon, reaching 4% of the 1748.9 $cm^{-1}$ FeNO absorption intensity. Broadband irradiation decreased the 1748.9 $cm^{-1}$ FeNO absorption and tripled the 1343.8 $cm^{-1}$ Fe[NO] absorption, showing that this photoisomerization is a favorable process.

$$\mathrm{FeNO}\ (^2\Delta) \xrightarrow{\mathrm{UV}} \mathrm{Fe[NO]}\ (^2\mathrm{A}') \qquad (10)$$

Note that 470−580 nm radiation initiated the analogous photoisomerization in Fe(CO)(NO) to the side-bound nitrosyl form Fe(CO)[NO].[34] A weak band at 1337.4 $cm^{-1}$ in solid nitrogen is apparently due to the Fe[NO] species.[72] Recent BP86 calculations predicted a $^2A'$ ground state for Fe[NO] 20.4 kcal/mol higher in energy than $^2\Delta$ FeNO and the N−O stretching frequency at 1271.0 $cm^{-1}$, which is lower than the observed value; apparently, other low-energy configurations contribute to the ground state of Fe[NO].[67,73]

Laser-ablated ruthenium and osmium reacted with nitric oxide to give the expected $M(NO)_{1-3}$ nitrosyl complexes.[74] The insertion products NMO observed for both metals differ in their stability relative to MNO; NOsO is more stable than OsNO, whereas the reverse is true for RuNO and NRuO. The M[NO] complexes were not observed. BPW91 calculations effectively reproduced the experimental observations and predicted frequencies of chemically useful accuracy using the LANL2DZ pseudopotential.

## G. Co Group

Absorptions at 1761.0 and 620.1 $cm^{-1}$ observed on sample deposition for CoNO in laser-ablation Co + NO/Ar experiments increased together on lower temperature annealing and then decreased on higher temperature annealing giving way to 1737.6 and 1770.1 $cm^{-1}$ absorptions due to the $Co(NO)_2$ and $Co(NO)_3$ molecules (Figure 7).[67] The 1761.0 $cm^{-1}$ band shows typical nitrosyl N−O stretching isotopic ratios ($^{14}N^{16}O/{}^{15}N^{16}O$: 1.0215 and $^{15}N^{16}O/{}^{15}N^{18}O$: 1.0205),

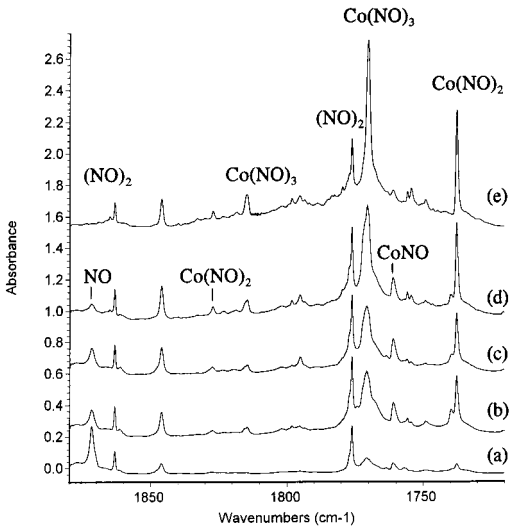


**Figure 7.** Infrared spectra in the 1880−1720 $cm^{-1}$ region from co-deposition of laser-ablated cobalt with 0.3% NO in argon: (a) after 1 h sample deposition at 10 K, (b) after annealing to 25 K, (c) after annealing to 30 K, (d) after annealing to 35 K, and (e) after annealing to 40 K.

while the 620.1 $cm^{-1}$ band exhibits isotopic ratios $^{14}N^{16}O/^{15}N^{16}O$: 1.0076 and $^{15}N^{16}O/^{15}N^{18}O$: 1.0267) that suggest a symmetric Co−N−O stretching mode. Although the mixed isotopic structure for the 1761.0 $cm^{-1}$ band is not clear due to band overlap in this region, a clear doublet is observed for the 620.1 $cm^{-1}$ band, which confirms that only one NO submolecule is involved. Ruschel et al.[25] assigned a 1767.2 $cm^{-1}$ band to CoNO and a 1760.6 $cm^{-1}$ band to the $Co_2NO$ molecule; however, no 1767 $cm^{-1}$ band was observed in laser-ablation experiments, and the preferential growth of strong $Co(NO)_2$ and $Co(NO)_3$ absorptions at the expense of the 1761.0 $cm^{-1}$ absorption verifies a single Co atom product. The 1761.0 and 620.1 $cm^{-1}$ bands were assigned by Zhou and Andrews to the CoNO molecule. The lack of $Co(NO)_3$ absorptions in the thermal Co experiments shows that the Co concentrations are relatively high and metal cluster species dominate. Although Co tends to dimerize in the absence of other reagents, the present observation of $Co(NO)_3$ demonstrates that the Co/NO ratio is substantially less in the laser-ablation experiments than in the previous thermal experiments.[25]

Previous DFT calculations predicted the CoNO molecule to have a triplet ground state with bent geometry.[14,25] Blanchet et al. discuss the competing bonding mechanisms in the singlet-linear and bent-triplet states.[14] Although B3LYP calculation finds the $^3A''$ state 7.6 kcal/mol lower in energy, the calculated N−O and Co−NO stretching frequencies are too low to fit the experimental values; however, BP86 calculation predicted the linear $^1\Sigma^+$ state 6.3 kcal/mol more stable than the $^3A''$ state and N−O and Co−NO stretching vibrational frequencies at 1832.0 and 704.5 $cm^{-1}$. Of at least equal importance, the BP86 calculated $^1\Sigma^+$ isotopic frequency ratios (14/15: 1.0225, 1.0067; 16/18: 1.0202, 1.0284) fit the experimental values (14/15: 1.0215, 1.0076; 16/18: 1.0205, 1.0267) much better than the calculated $^3A''$ state isotopic frequency ratios (14/15: 1.0199, 1.0176; 16/18: 1.0253, 1.0133). This normal mode description points to a linear $^1\Sigma^+$ ground state for the CoNO molecule.[67] Note that the lower frequency mode is more structure sensitive and that the isoelectronic NiCO and $NiNO^+$ species have $^1\Sigma^+$ ground states.[19,67] We believe that a higher level calculation will find a $^1\Sigma^+$ ground state for CoNO.

The 1737.6 $cm^{-1}$ band assigned to $Co(NO)_2$ increased markedly on annealing, and a clear triplet with approximately 1:2:1 relative intensities was observed in the mixed $^{14}N^{16}O + ^{15}N^{16}O$ experiments, which is appropriate for the antisymmetric N−O stretching vibration of the $Co(NO)_2$ molecule with two equivalent NO subunits. A weak band at 1827.2 $cm^{-1}$ tracked with the 1737.6 $cm^{-1}$ band and is assigned to the symmetric N−O stretching vibration mode. The weak combination band at 3524.8 $cm^{-1}$, which is 40.0 $cm^{-1}$ below the sum of fundamentals, supports these assignments. The antisymmetric N−O stretching vibration of the $Co(NO)_2$ molecule is observed at 1749.1 $cm^{-1}$ in neon. Recent BP86 calculation predicted a $^2B_1$ ground state for $Co(NO)_2$ with antisymmetric and symmetric N−O stretching vibrations at 1767.3 and 1836.7 $cm^{-1}$. The weight of evidence with both symmetric and antisymmetric N−O stretching fundamentals and their combination band confirms this spectroscopic identification of $Co(NO)_2$.[67]

Four bands at 1814.6, 1770.1, 579.3, and 493.8 $cm^{-1}$ increased together on annealing in solid argon. The two upper bands exhibited N−O stretching frequency ratios. The two lower bands showed large $^{14}N^{16}O/^{15}N^{16}O$ ratios (1.0233 and 1.0251) and small $^{15}N^{16}O/^{15}N^{18}O$ ratios (1.0041 and 1.0061), indicating that these two bands belong to Co−NO stretching vibrations. In the mixed $^{14}N^{16}O + ^{15}N^{16}O$ experiment, clear quartets were observed for the 1770.1, 579.3, and 493.8 $cm^{-1}$ bands, indicating that three equivalent NO submolecules are involved in these vibrational modes. Following the $Fe(NO)_3$ molecule, these four bands are assigned to the symmetric and antisymmetric N−O and Co−NO stretching vibrations of the $Co(NO)_3$ molecule with $C_{3v}$ symmetry.[67] The assignments were strongly supported by DFT calculations, which predict a $^1A_1$ ground state with symmetric and antisymmetric N−O and Co−NO stretching vibrations at 1886.2, 1796.0, 595.2, and 531.7 $cm^{-1}$, in good agreement with experimental values. The compound $Co(NO)_3$ with nearly linear CoNO linkages is of some interest as a closed-shell 18-electron transition metal nitrosyl since the chromium compound $Cr(NO)_4$ is the only transition metal nitrosyl yet isolated in pure form.[36]

New 1284.2 and 1317.4 $cm^{-1}$ absorptions were assigned to the Co-($\eta^2$-NO) complex in solid argon and neon, respectively. This mode was calculated at 1341.8 (BP86) and 1394.5 $cm^{-1}$ (B3LYP) in its $^1A'$ ground state, which are 16.8 kcal/mol (BP86) and 13.2 kcal/mol (B3LYP) higher than energies calculated for the $^1\Sigma^+$ CoNO molecule.[67] The 1284.2 $cm^{-1}$ Co[NO] band increases on photolysis and on annealing, reaching half the absorbance of the 1761.0 $cm^{-1}$ CoNO band.

Laser-ablated rhodium and iridium atoms reacted with nitric oxide and formed the nitrosyl complexes $Rh(NO)_{1-3}$ and $Ir(NO)_{1-3}$ as main products.[75] In

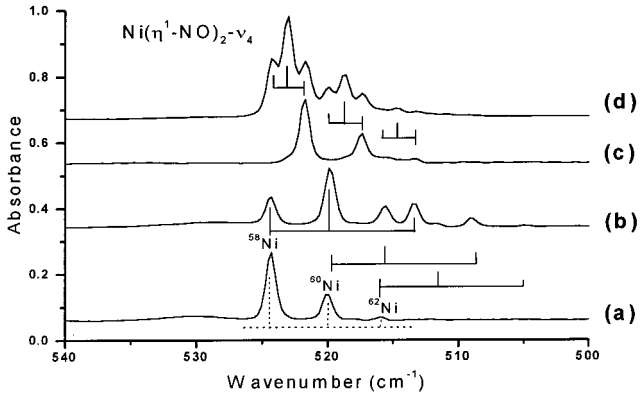


**Figure 8.** Infrared spectra in the 540−500 $cm^{-1}$ region for Ni-($\eta^1$-NO)$_2$ using isotopic NO precursors at 1% concentration with 0.5% Ni after annealing to 35 K: (a) $^{14}N^{16}O$, (b) $^{14}N^{16}O + {}^{14}N^{18}O$, (c) $^{15}N^{16}O$, and (d) $^{14}N^{16}O + {}^{15}N^{16}O$. (Figure courtesy of L. Manceron.)

contrast to Co, the inserted NRhO and NIrO molecules were observed. DFT calculations for these products using the BPW91 and B3LYP functionals determine frequencies with the same accuracy found for other metal nitrosyls and are a useful predictive tool.[75]

## H. Ni Group

The end-bound NiNO complex has been studied in benchmark work by the Paris group, and the overtone and N−O and Ni−NO stretching vibrational modes were reported at 3324.3, 1677.1, and 608.4 $cm^{-1}$ in solid argon.[28] The earlier thermal report[25] assigned two bands to NiNO: the Paris study showed that the 1727.3 $cm^{-1}$ band arises from NNNiNO, and only the band at 1676.2 $cm^{-1}$ is due to NiNO.[28] Similar bands at 3323.7, 1676.6, and 608.5 $cm^{-1}$ in laser-ablation experiments are due to the NiNO molecule.[67] The 1676.6 and 608.5 $cm^{-1}$ bands are 30:1 relative absorbance. The resolved $^{58}$NiNO and $^{60}$NiNO components at 608.5 and 605.2 $cm^{-1}$ clearly show that a single Ni atom is involved in this vibrational mode and molecular species. Although earlier CASSCF calculations suggested a linear NiNO molecule,[76] recent DFT calculations predicted a $^2$A′ ground state for NiNO with bond angle around 140° and nitrosyl frequencies in the 1660 to 1699 $cm^{-1}$ range.[14,25,28,67,77] The two modes were calculated at 1703.9 and 644.8 $cm^{-1}$ and 42:1 relative intensity with BP86 and at 1726.0 and 518.3 $cm^{-1}$ and 22:1 relative intensity with B3LYP.[67] The Paris group compared four density functionals and found the best agreement (1684.4 $cm^{-1}$) for the pure BPW91 density functional.[28]

Bands at 3555.2, 1749.7, 524.4, and 520.2 $cm^{-1}$ in argon matrix experiments increased on annealing. The weak 3555.2 $cm^{-1}$ band also shifted with $^{15}$NO and $^{15}N^{18}O$ appropriately for a N−O stretching mode. The 1749.7 $cm^{-1}$ band exhibited N−O stretching vibrational ratios, and triplets were presented in the mixed experiments. The 524.4 and 520.2 $cm^{-1}$ bands exhibited the intensity distribution appropriate for natural abundance $^{58}$Ni and $^{60}$Ni, clearly indicating one Ni atom involvement.[67] The Manceron group obtained a higher product yield and also observed the weaker $^{62}$Ni component, as shown in Figure 8, and a much weaker 623.9 $cm^{-1}$ absorption for the bending mode.[78] The 3552.5 $cm^{-1}$ absorption is assigned to the combination band of symmetric and antisymmetric N−O stretching modes, and the 1749.7 and 534.4 $cm^{-1}$ bands to the antisymmetric N−O and Ni−NO stretching vibrations of the Ni(NO)$_2$ molecule. The difference 3555.2 − 1749.7 = 1805.5 $cm^{-1}$, with correction for anharmonicity, is reasonable for the symmetric N−O stretching mode. The N−O stretching combination and fundamental were observed at 3572.8 and 1759.9 $cm^{-1}$ in solid neon.[67] A recent BP86 calculation predicted a linear Ni(NO)$_2$ molecule, a $^3\Sigma_g^-$ ground state, and symmetric and antisymmetric N−O and Ni−NO stretching frequencies at 1848.7, 1777.3, and 533.8 $cm^{-1}$, and a B3LYP computation gave 1883, 1820, and 559 $cm^{-1}$ values.[67,78] The linear geometry from DFT is consistent with the absence of the symmetric N−O mode in the infrared spectrum.

The N−O stretching vibration of the side-bound isomer Ni[NO] was observed at 1293.7 $cm^{-1}$ in argon and at 1292.6 $cm^{-1}$ in neon.[28,67] Both NiNO and Ni[NO] increase on annealing solid argon to 25 K. It is interesting to note that Manceron et al. observed reversible photoisomerism between the two isomers:

$$\mathrm{NiNO}\ (^2\mathrm{A}') \underset{436\ \mathrm{nm}}{\overset{240\ \mathrm{nm}}{\rightleftharpoons}} \mathrm{Ni[NO]}\ (^2\mathrm{A}'') \qquad (11)$$

BP86 calculations predicted a $^2$A″ ground state for Ni-($\eta^2$-NO), which is 20.5 (BP86) and 11.6 kcal/mol (B3LYP) higher in energy than the $^2$A′ NiNO molecule, and a N−O stretching vibrational frequency at 1313.4 (BP86) and 1374.7 $cm^{-1}$ (B3LYP).[67] The Paris group obtained a higher yield of Ni[NO] and also observed the weaker ring-stretching modes at 540.5 and 464.4 $cm^{-1}$ in excellent agreement with their BPW91 calculated values.[28] It must be noted that BP86 and BPW91 (1297.9 $cm^{-1}$) predict nearly the same N−O stretching frequencies, but the lowest frequency Ni−O mode is better modeled by the later version of the functional.[28] The side-bonded M[NO] species with TM−O and TM−N bonds are clearly the most difficult to describe theoretically. The Ni[NO] complex is related to the photogenerated [Ni($\eta^2$-NO)($\eta^5$-Cp*)] species,[6] but we note that measured N−O bond length in the latter (1.134 Å) is much shorter than calculated for Ni[NO], namely 1.276 Å (BPW91) or 1.252 Å (B3LYP).[28,67]

The Manceron group employed higher NO concentrations and observed the bis-side-bound Ni[NO]$_2$ species at 1343.9 $cm^{-1}$. The crucial isotopic spectra which identify this species are shown in Figure 9 where the mixed isotopic triplets confirm the participation of two equivalent NO subunits.[78] Recent B3LYP calculations found a doubly bridging form in the $^1$A$_1$ ground state with almost parallel NO ligands, a +65 kcal/mol total binding energy, and a strong 1471 $cm^{-1}$ b$_2$ mode. This may be compared with a +96 kcal/mol total binding energy for $^3\Sigma_g^-$ Ni(NO)$_2$. These workers converted the bis-ring form to the bis-linear form with 405 nm irradiation. The bis-ring structure is energetically stable as it can be formed on matrix annealing and NO diffusion at the expense of the mononitrosyl species.[78]

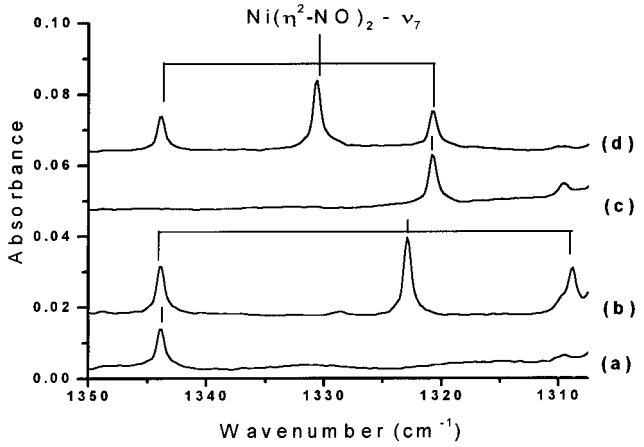


**Figure 9.** Infrared spectra in the 1350−1310 $cm^{-1}$ region for Ni-($\eta^2$-NO)$_2$ using isotopic NO precursors at 1% concentration with 0.5% Ni: (a) $^{14}N^{16}O$, (b) $^{14}N^{16}O + {}^{14}N^{18}O$, (c) $^{15}N^{16}O$, and (d) $^{14}N^{16}O + {}^{15}N^{16}O$. (Figure courtesy of L. Manceron.)

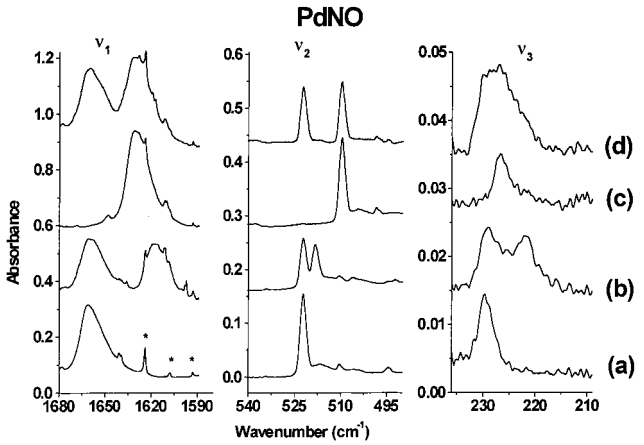


**Figure 10.** Infrared spectra in the fundamental regions for PdNO. (a) Pd/$^{14}N^{16}O$/Ar = 0.5/1/100, (b) same with ($^{14}N^{16}O/^{14}N^{18}O$ = 0.6/0.4), (c) same with $^{15}N^{16}O$, (d) same with ($^{14}N^{16}O + {}^{15}N^{16}O$ = 0.55/0.45). The asterisks designate water impurity lines. (Figure courtesy of L. Manceron.)

Laser-ablated Pd and Pt atoms interact with NO to form M(NO)$_{1,2}$ in excess argon and neon without evidence of the M[NO] species.[79] Recent thermal work obtained similar results.[80] Again with higher yields the Pd−N stretching mode so important to understanding the metal−nitrogen bond was observed at 522.1 $cm^{-1}$ and the Pd−N−O bending mode at 229.8 $cm^{-1}$. Figure 10 illustrates isotopic spectra of these three fundamentals with very different intensities.[80] The thermal work also obtained a higher yield of Pd(NO)$_2$ and observed far-IR modes at 494.5 and 433.5 $cm^{-1}$.

The Paris group performed a population analysis of PdNO, NiNO, and Ni[NO].[80] These results indicate a decrease in N−O bonding from $\eta^1$ to $\eta^2$ with nickel but an increase for $\eta^1$ bonding to palladium. It is interesting to note that the metal contribution in the metal−ligand bond varies as the binding energy. In the most stable complex NiNO ($\eta^1$), the metal contribution in the metal−ligand bond is 0.66 e whereas it is only 0.35 e in the Ni[NO] ($\eta^2$). In the PdNO ($\eta^1$) case, palladium participates with 0.36 e in the Pd−N bond. The binding energies are NiNO, 36.5 kcal/mol, Ni[NO], 24.1 kcal/mol, and PdNO, 30.3 kcal/mol. Finally, the Paris group explored the potential energy surface for evidence of Pd[NO] and found none, which supports the failure to detect this species in both laboratories.

Smith and Carter performed GVB(4/8)-PP calculations and predicted $^2A'$ ground states[81] and 1686 and 1775 $cm^{-1}$ modes for PdNO and PtNO in agreement with the recent DFT results. However, due to atomic promotional costs, they suggested that $^2\Pi$ with a 1866 $cm^{-1}$ computed frequency should be the ground state of PdNO. Clearly, the 1866, 524, and 99 $cm^{-1}$ computed frequencies are not compatible with the PdNO matrix absorptions, but the 1686, 671, and 292 $cm^{-1}$ frequencies calculated for the $^2A'$ ground state are in agreement with the matrix spectrum described above. Furthermore, Alikhani et al. find an imaginary bending frequency for the $^2\Pi$ Renner−Teller state.[78] Hence, $^2A'$ is the ground state of PdNO based on agreement between three observed and calculated frequencies. Finally, we note that Smith and Carter describe the computed 292 $cm^{-1}$ band as the Pd−N stretching mode and the 671 $cm^{-1}$ band as the Pd−N−O bending mode.[81] These two modes are, of course, mixed for a bent molecule, but the BPW91 calculated frequencies at 1700.1, 533.8, and 256.9 $cm^{-1}$ show displacements that describe the 533.8 $cm^{-1}$ band as predominantly a Pd−N stretching mode. Furthermore, the observed isotopic frequency ratio $^{14}NO/^{15}NO$ = 522.1/509.6 = 1.02453 is nearly that for a pure Pd−N stretching mode (1.03068), which shows that the 522.1 $cm^{-1}$ absorption is better described as "the Pd−N stretching mode".

Although this review is not intended to cover metal cluster nitrosyls, metal clusters are important as small molecules react with TM clusters in a manner analogous to the extended metal surface.[82] Therefore, it is interesting to compare the nickel group MNO and (M$_2$)NO species particularly in view of recent DFT calculations on such species by Duarte and Salahub, which predict the N−O fundamental in (Ni$_2$)NO to be 135 $cm^{-1}$ lower than in NiNO at the GGA-PP level.[77] New absorptions have been observed at 1503.8, 1504.2, and 1522.6 $cm^{-1}$ in Ni, Pd, and Pt experiments that show a second-order metal and first-order NO dependence.[79,80] In particular, mixed isotopic doublets for one NO subunit were observed. These bands fall, respectively, 172.8, 157.6, and 154.4 $cm^{-1}$ below the MNO values, in very good agreement with the DFT differences (BP86, 183.0; BPW91, 159.5; BPW91, 162.2 $cm^{-1}$). Duarte and Salahub predicted the linear doublet NiNiNO species 6.0 kcal/mol higher in energy, but did not calculate its frequencies. Citra and Andrews found a nearly linear $^2A'$ NiNiNO species to be only 0.7 kcal/mol higher and to have a strong 1807.5 $cm^{-1}$ stretching frequency,[79] which is near new absorptions that appear on annealing in the Ni/NO sample at 1802.6, 1808.4, and 1813.5 $cm^{-1}$. Similarly, a bent $^2A'$ PdPdNO species is found 9 kcal/mol higher than (Pd$_2$)NO, which is the same energy ordering reported previously,[83] and the former has a very strong calculated 1763.5 $cm^{-1}$ absorption.[79] However for platinum, the linear PtPtNO ($^2\Sigma^+$) species is found to be 23 kcal/mol lower

than $(Pt_2)NO$ ($^2A'$) and to exhibit a very strong 1864.4 $cm^{-1}$ absorption. Evidence was also observed for the PdPdNO and PtPtNO species in recent argon matrix experiments.[79] Apparently both open and bridged forms can be trapped in the low-temperature matrix.

## I. Cu Group

Thermal copper atom reactions with NO were first reported by Chiarelli and Ball: these workers assigned new 1610.5 and 608.8 $cm^{-1}$ bands to the N−O and Cu−N stretching vibrations of CuNO and a weaker 1586.0 $cm^{-1}$ band to $Cu(NO)_2$.[23] However, mixed $^{14}NO + {}^{15}NO$ isotopic spectra recorded using laser-ablated copper atoms showed the former bands as 1:2:1 triplets characteristic of two equivalent NO subunits and the latter band as a 1:1 doublet for the vibration of a single NO subunit, and hence, the original assignments must be reversed.[84] In the laser-ablation argon matrix experiments, the antisymmetric N−O stretching vibration of $Cu(NO)_2$ was observed at 1611.6 $cm^{-1}$ with a combination band at 3373.2 $cm^{-1}$, which by difference gives the symmetric N−O stretching frequency at 1761.6 $cm^{-1}$, and the CuNO fundamental was found at 1587.1 $cm^{-1}$.

The corresponding neon matrix spectra[84] are illustrated in Figure 11A,B. The neon matrix blue shifts CuNO to 1602.2 $cm^{-1}$ and $Cu(NO)_2$ to 1637.2 $cm^{-1}$. Note the 1:2:1 triplet isotopic structure for the $Cu(NO)_2$ fundamental and combination bands with the same band profile splittings for each feature and the increase in $Cu(NO)_2$ at the expense of CuNO on annealing the solid neon matrix to 12 K. The Cu + NO reaction is exothermic by 10.4 kcal/mol at the CCSD(T) level of theory,[44] and this reaction proceeds on annealing in both solid argon and neon.

Copper has too many electrons to form a trinitrosyl like cobalt, but there is evidence for a $Cu(NO)_2(NO)^*$ species with two equivalent nitrosyls and a third inequivalent NO subunit. The sextet mixed-isotopic pattern in Figure 11B is characteristic of such a species. DFT calculations suggested that the (NO)* subunit is bent rather than side-bound.[84]

CuNO has been the subject of several theoretical studies. Hrušák and co-workers found that a $^3A''$ state is more stable than the $^1A'$ state at the SCF, CISD, and CCSD level of theory, while the CCSD(T) method convincingly shows that the $^1A'$ state is the ground state.[44] Blanchet and co-workers also predicted a $^1A'$ ground state for CuNO using the DFT method.[14] Recent DFT calculations found the $^1A'$ state 2.9 kcal/mol lower in energy than the $^3A''$ state using BP86, but they found the $^3A''$ state 3.1 kcal/mol lower in energy using the B3LYP functional.[84] As has been discussed in detail, both $^1A'$ and $^3A''$ states have bent structures.[14] The $^3A''$ state CuNO was predicted to have a longer N−O bond, and hence, a lower N−O stretching frequency. The calculated energies and frequencies are close for both states, which makes it difficult to determine which state is the ground state. The observed N−O isotopic frequency ratios for $^{14}N^{16}O/^{15}N^{16}O$ (1.0175) and $^{15}N^{16}O/^{15}N^{18}O$ (1.0278) are in excellent agreement with the ratios observed for NO itself (1.0179 and 1.0277) and show little N−O interaction with the Cu−N vibrational mode in contrast to $Cu(NO)_2$ discussed below. However, the lower frequency modes are more diagnostic of the state, and Manceron et al. have recently observed weak 452.6 and 278.2 $cm^{-1}$ absorptions that track with the strong 1587.4 $cm^{-1}$ fundamental for CuNO in solid argon.[85] This is significant because these three fundamentals, and most importantly the $^{65}Cu$, $^{15}N$, and $^{18}O$ isotopic frequencies of the 452.6 $cm^{-1}$ mode, are in very good agreement with DFT calculations for the $^1A'$ state but in poor agreement with similar computations for the $^3A''$ state. This agreement coupled with observation of the two higher frequency modes in solid neon at 1602.2 and 452.1 $cm^{-1}$ confirm that $^1A'$ is the CuNO ground state.[85]

DFT calculations also substantiate the $Cu(NO)_2$ assignment.[84] At the BP86/6-311+G* level of theory, linear $^2\Pi_u$ and bent $^4A_2$ states are found to be nearly

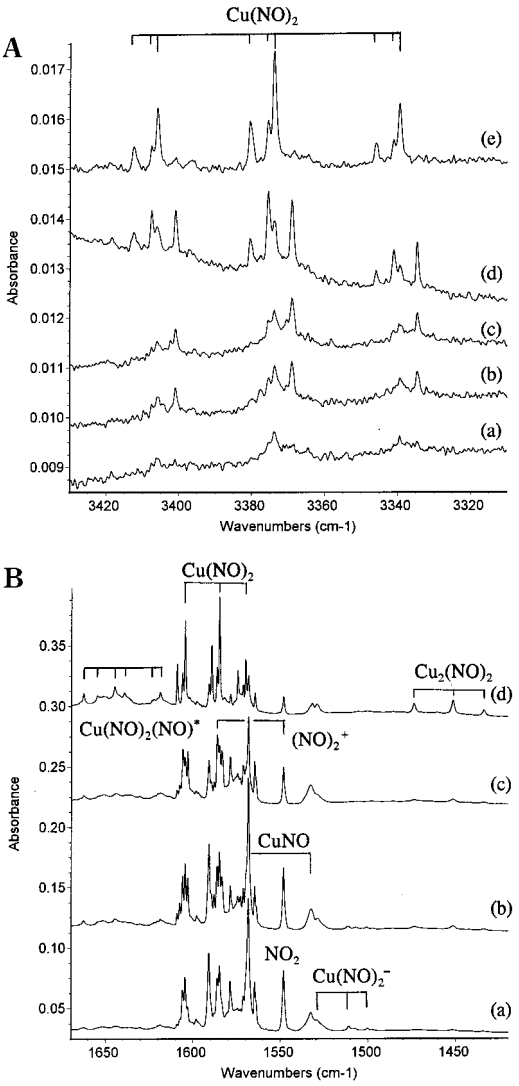


**Figure 11.** (A) Infrared spectra in the 3430−3310 $cm^{-1}$ region for laser-ablated copper atoms co-deposited with $0.05\%^{14}N^{16}O + 0.05\%^{15}N^{16}O$ in neon: (a) after 45 min sample deposition at 4 K, (b) after annealing to 8 K, (c) after 15 min full arc photolysis, (d) after annealing to 10 K, and (e) after annealing to 12 K. (B) Infrared spectra in the 1670−1420 $cm^{-1}$ region for laser-ablated copper atoms co-deposited with $0.05\%^{15}N^{16}O + 0.05\%^{15}N^{18}O$ in neon: (a) after 45 min sample deposition at 4 K, (b) after annealing to 8 K, (c) after 15 min full arc photolysis, and (d) after annealing to 12 K.

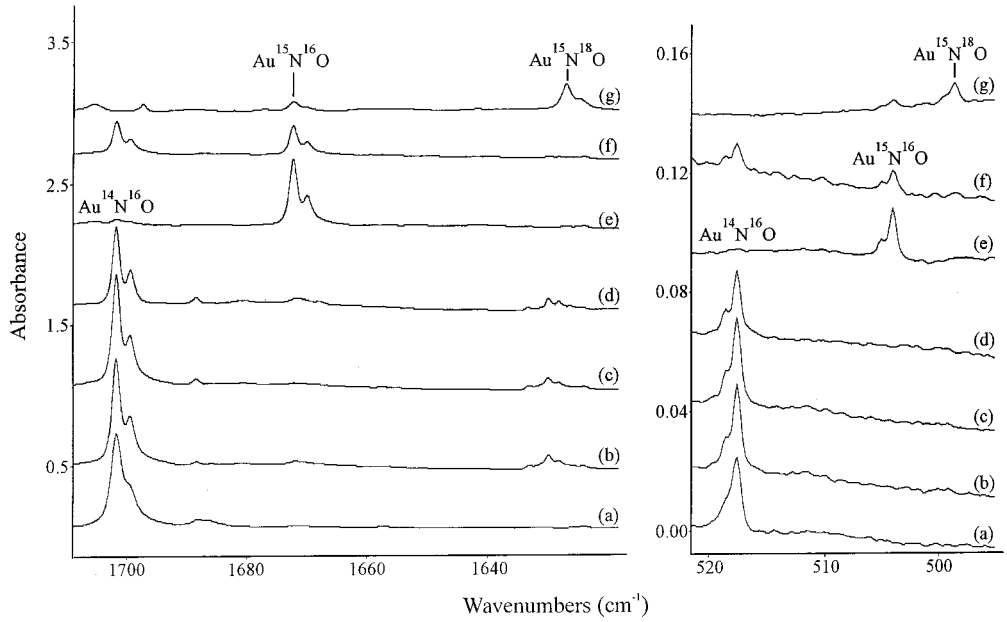


**Figure 12.** Infrared spectra in the 1710−1610 and 520−490 $cm^{-1}$ regions for laser-ablated gold atoms and nitric oxide: (a) after 60 min deposition with 0.3% NO in argon at 7 K, (b) annealing to 25 K, (c) 25 min irradiation, $\lambda > 240$ nm, (d) annealing to 30 K, (e) after 60 min deposition with 0.2% $^{15}N^{16}O$ in argon and annealing to 25 K, (f) 60 min deposition with 0.15% NO and 0.15% $^{15}N^{16}O$ in argon after annealing to 25 K, and (g) 60 min deposition with 0.3% $^{15}N^{18}O$ and 0.1% $^{15}N^{16}O$ in argon after annealing to 25 K.

identical in energy, and a bent $^2B_1$ state is about 15.3 kcal/mol higher in energy. The $^2\Pi_u$ state exhibited shorter Cu−N and N−O bond lengths than the $^4A_2$ state and gave higher N−O and Cu−NO stretching vibrational frequencies. At the B3LYP/6-311+G* level of theory, a linear quartet state is predicted to be the most stable, with the linear $^2\Pi_u$ and the bent $^2B_1$ states lying 15.6 and 27.0 kcal/mol higher in energy. The calculated frequencies for the $^2\Pi_u$ state fit the experimental values much better, and both functionals compute the symmetric N−O stretching and antisymmetric Cu−NO stretching vibrational frequencies of the quartet state too low. These comparisons strongly suggest a $^2\Pi_u$ ground state for the $Cu(NO)_2$ molecule. Finally, calculations found the antisymmetric ON−Cu−NO stretching mode near 600 $cm^{-1}$ for the $Cu(NO)_2$ molecule and further confirmed the reassignment since the Cu−NO vibration for CuNO is predicted below 500 $cm^{-1}$. In addition, both functionals (BP86, B3LYP) compute isotopic frequencies with ratios (1.0208, 1.0206 for $^{14}N^{16}O/^{15}N^{16}O$ and 1.0232, 1.0236 for $^{15}N^{16}O/^{15}N^{18}O$) that effectively model the vibrational coupling evidenced in the antisymmetric N−O stretching mode of linear ON−Cu−NO, which is different from that in CuNO. The reaction of CuNO with another NO molecule proceeds readily on annealing, and the exothermic (−36.9 kcal/mol, BP86) reaction is expected from the shorter Cu−N bonds in $Cu(NO)_2$ as compared to CuNO.

Silver and gold react with NO to form bent metal nitrosyls with N−O frequencies at 1680.2 and 1707.3 $cm^{-1}$ in solid argon and neon for silver and at 1701.9 and 1710.4 $cm^{-1}$ for gold.[86,87] The yield of AuNO was sufficient to observe the weaker Au−N stretching mode at 517.8 $cm^{-1}$, which exhibits a $^{14}NO/^{15}NO$ ratio 1.0274 that approaches the Au−N diatomic ratio (1.0325) (Figure 12) and also the N−O overtone at 3372.5 $cm^{-1}$. DFT does a very good job of predicting both stretching fundamentals of $^1A'$ ground state AuNO.[87] Gold also forms a strong $Au(NO)_2$ complex, but silver does not; in contrast, silver gives an AgONNO species with significant charge-transfer character, but the 1387.5 $cm^{-1}$ frequency is still not as low as that for the isolated $(NO)_2^-$ anion (1222 $cm^{-1}$).[88] The hyponitrite complex $Ag(NO)_2Ag$ is the major product with strong absorptions at 1121.1 and 1185.5 $cm^{-1}$ in the above matrices,[85] which approach the 1030 $cm^{-1}$ solid hyponitrite and 1028.5 $cm^{-1}$ matrix-isolated hyponitrite values.[88]

## *IV. Charged Binary Transition Metal Nitrosyls*

Nitrosyl cations and anions are more difficult to study than the neutral species because they are more reactive, and the anions are likely to be sensitive to photodetachment. Experimental work on nitrosyl cations in the gas phase is limited to a few mass spectroscopic investigations, which provide a range of bond dissociation energies for several $Fe^+$, $Co^+$, $Ni^+$, and $Cu^+$ species.[89−92] Gas-phase studies of TM nitrosyl anions are lacking for want of a stable precursor. Both TM nitrosyl cations and anions can be prepared from laser-ablated TM atoms, cations, and electrons as recently demonstrated for TM carbonyl cations and anions in our laboratory.[20−22] The spectra of TM-carbonyl cations, neutrals, and anions have been compared in a recent review.[93] Cations and anions are unique to laser-ablation experiments as thermal evaporation produces only neutral species. Recently, Van Zee and Weltner have reported ESR spectra of the $Ni^+$, $Pd^+$, and $Pt^+$ radical cations in solid argon using laser ablation of the metal targets.[94] Clearly, laser ablation also produces metal cations and electrons, and both must be considered as reagents in matrix-isolation experiments.

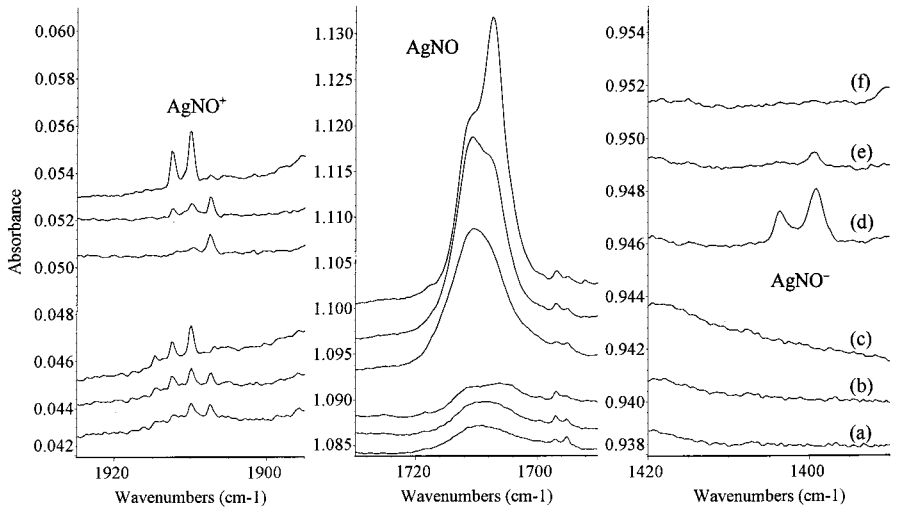


**Figure 13.** Infrared spectra in the 1925−1895, 1730−1690, and 1420−1390 $cm^{-1}$ regions for laser-ablated silver and NO in excess neon: (a) 0.2% NO and 0.02% $CCl_4$ in neon co-deposited for 25 min at 5 K, (b) after annealing to 8 K, and (c) after annealing to10 K, (d) 0.1% NO in neon co-deposited for 50 min at 5 K, (e) after annealing to 8 K, and (f) after annealing to10 K.

Figure 13 illustrates spectra for $AgNO^{+,0,-}$ and contrasts the effect of adding $CCl_4$ to the matrix sample.[86] First, the major bands on silver and NO deposition, Figure 13d, are 1907.5, 1711.8, and 1399.2 $cm^{-1}$, and the relative integrated intensities of the three bands are 1:100:5, respectively; the ablated material is mostly atoms with a few percent cations and electrons. Next, annealing to 8 and 10 K destroys the anion band, increases AgNO with dominant absorption at 1707.3 $cm^{-1}$, and increases $AgNO^+$ matrix site absorptions at 1909.9 and 1912.4 $cm^{-1}$. On sample deposition with added $CCl_4$, Figure 13a, there is no $AgNO^-$, and approximately the same $AgNO^+$ absorption with 20% as much AgNO. The $AgNO^+$/AgNO ratio is 5 times greater with $CCl_4$ added to capture ablated electrons, which prevents the formation of $AgNO^-$ and increases the relative amount of $Ag^+$ present.

Hence, the $CCl_4$-doped sample experiments, along with DFT frequency calculations, conclusively identifiy TM cation and anion nitrosyl species. The TM nitrosyl cations are produced here by the direct reaction of NO with ablated cations, and the TM anions through electron capture by neutral nitrosyls, reactions 12 and 13.[22,86]

$$Ag^+ + NO \rightarrow AgNO^+ \quad (12)$$

$$AgNO + e^- \rightarrow AgNO^- \quad (13)$$

## A. Early TM Nitrosyl Cations

In the scandium experiments, a weak 1117.0 $cm^{-1}$ absorption decreased on annealing and ultraviolet irrradiation and increased substantially on $CCl_4$ doping. Isotopic mixtures characterized a single NO oscillator with unusual $^{14}N^{16}O/^{15}N^{16}O$ (1.01527) and $^{15}N^{16}O/^{15}N^{18}O$ (1.02842) frequency ratios, which indicated less nitrogen and more oxygen participation than in NO itself and the opposite behavior from most nitrosyls. Assignment to $Sc[NO]^+$ is supported by BP86 calculation of the ground state $^2A''$ cation with strong 1146.9 $cm^{-1}$ fundamental and 1.01658 and 1.02919 isotopic frequency ratios. This excellent agreement verifies the observation of $Sc[NO]^+$ in solid argon.[59] The $Sc[NO]^+$ cation is made by the direct reaction of laser-ablated $Sc^+$ and NO. The role of $CCl_4$ is to capture ablated electrons and allow $Sc^+$ and $Sc[NO]^+$ to survive the deposition process.

Thomas et al. reported a systematic study of first-row TM nitrosyl cations.[15] These workers find side-bonded ground states for the first three metals and a 1158.2 $cm^{-1}$ B3LYP frequency for $Sc[NO]^+$, which is almost the same as the BP86 frequency. However, cyclic $V[NO]^+$ is only 0.6 kcal/mol more stable than linear $VNO^+$ at the CCSD(T) level.[15] This led Zhou and Andrews to assign tentatively a very weak 1720.4 $cm^{-1}$ band to $VNO^+$ in solid argon.[63] The argon matrix experiment was repeated with $CCl_4$ added, and the 1720.4 $cm^{-1}$ band was not enhanced, but a weak 1137.0 $cm^{-1}$ band was increased 4-fold relative to the 1075.7 $cm^{-1}$ V[NO] absorption. Hence, the 1137.0 $cm^{-1}$ feature is $V[NO]^+$ in solid argon, and the corresponding neon matrix band at 1143.7 $cm^{-1}$ exhibits a typical blue shift.[66]

## B. Late TM Nitrosyl Cations

The nitrosyl vibrations observed for 15 late TM nitrosyl cations in solid neon are listed in Table 2. These absorptions generally increased on lower temperature annealing, disappeared on ultraviolet irradiation, and increased relative to MNO on $CCl_4$ doping. The isotopic spectra in Figure 14 reveal mixed-isotopic doublets for $NiNO^+$ and verify a single NO vibrator. The linear ground states found for the Fe, Co, and Ni nitrosyl cations with B3LYP were matched by BP86, and the frequencies calculated using both functionals are slightly higher than the observed values.[67] Both calculations determined $CuNO^+$ to be bent ($^2A'$) and predicted a frequency compatible with experiment.[84] The bent $CuNO^+$ structure obtained by DFT is in agreement with earlier higher level calculations, but more recent work has refined the bond distances.[15] These DFT calculations[15] also show that the $^2\Pi$ state, claimed

**Table 2. Vibrational Stretching Frequencies ($cm^{-1}$) Observed for Binary Unsaturated Transition Metal Nitrosyl Cations and Anions in Solid Neon and Argon[a]**

| cations | Ne | Ar | ref | anions | Ne | Ar | ref |
|---|---|---|---|---|---|---|---|
| $Sc[NO]^+$ | 1159.9 | 1117.0 | 59 | $CrNO^-$ | 1519.9 | 1511.5 | 26, 66 |
| $V[NO]^+$ | 1143.7 | 1137.0 | 66 | $Cr(NO)_2^-$ | | 1463.1 | 26 |
| $FeNO^+$ | 1897.3 | | 67 | $Cr(NO)_3^-$ | 1557.8 | 1548.9 | 26, 66 |
| $RuNO^+$ | 1918.0 | | 74 | $CoNO^-$ | 1585.7 | | 67 |
| $OsNO^+$ | 1921.8 | 1901.5 | 74 | $Co(NO)_2^-$ | 1593.8 | | 67 |
| $CoNO^+$ | 1957.5[b] | | 67 | $NiNO^-$ | 1454.7 | 1443.4 | 67 |
| $Co(NO)_2^+$ | 1902.7[b] | | 75 | $Ni(NO)_2^-$ | 1592.2 | | 67 |
| $RhNO^+$ | 1957.5 | | 75 | $PdNO^-$ | 1487.6 | | 79 |
| $IrNO^+$ | 1990.0 | | 75 | $PtNO^-$ | 1462.1 | | 79 |
| $NiNO^+$ | 2001.9 | | 67 | $Cu(NO)_2^-$ | 1565.2 | 1551.2 | 84 |
| $Ni(NO)_2^+$ | 1926.2 | | 67 | $AgNO^-$ | 1399.2 | 1392.3 | 85 |
| $PdNO^+$ | 1924.0 | 1921.6 | 79 | | | | |
| $PtNO^+$ | 2019.6 | 2010.4 | 79 | | | | |
| $CuNO^+$ | 1907.9 | | 84 | | | | |
| $AgNO^+$ | 1909.9 | 1904.3 | 85 | | | | |
| $AuNO^+$ | 1917.8 | | 86 | | | | |
| $Au(NO)_2^+$ | 1895.7 | | 86 | | | | |

[a] Cations enhanced and anions markedly decreased with $CCl_4$ added. [b] Although $Co^{14}N^{16}O^+$ and $Rh^{14}N^{16}O^+$ have the same absorption in solid neon, the $^{15}N^{16}O$ (1919.0, 1919.9 $cm^{-1}$) and $^{15}N^{18}O$ isotopic cations (1874.7, 1874.1 $cm^{-1}$, respectively) are different. The different isotopic frequency ratios again indicate different metal−nitrogen mode mixing.

to be the ground state,[95] is actually a transition state between bent structures for ground state $CuNO^+$. Furthermore, high-level CCSD(T) calculations place the bent structure 2 kcal/mol below the linear structures.[15,44]

Going down the periodic table, the $PtNO^+$ frequency observed at 2019.6 $cm^{-1}$ in Figure 15 is slightly higher than the $NiNO^+$ fundamental. In each late group, the $MNO^+$ frequency increases on going down the group (Fe to Ru to Os) as the larger $M^+$ is less effective at back-bonding to NO. The exception is $PdNO^+$ where a substantial decrease was observed. However, both BPW91 and B3LYP functionals predict the $PdNO^+$ fundamental below that for $PtNO^+$ (76 and 68 $cm^{-1}$) which is near the experimental difference (96 $cm^{-1}$ in solid neon). Perhaps the reason is that $PdNO^+$ is bent in the ground state ($^1A'$, 135 ± 1°) like the Cu, Ag, Au nitrosyl cations, in contrast to $NiNO^+$ and $PtNO^+$, which are linear ($^1\Sigma^+$), and accordingly the $PdNO^+$ frequency is just 6−16 $cm^{-1}$ higher than the $CuNO^+$, $AgNO^+$, and $AuNO^+$ values. The earlier GVB (4/8)-PP calculations[81] predict both $PdNO^+$ and $PtNO^+$ to be bent ($^2A'$) whereas both density functionals find the $^1\Sigma^+$ linear ground state for $PtNO^+$. Furthermore, the BPW91 functional predicts a 2043.8 $cm^{-1}$ N−O frequency for $^1\Sigma^+$ $PtNO^+$, in excellent agreement with the 2019.6 $cm^{-1}$ neon matrix value,[79] whereas the $^1A'$ state prediction (1865 $cm^{-1}$) is not compatible.[81] Smith and Carter describe the different bonding interactions in these two $PdNO^+$ states: in the $^1A'$ state $PdNO^+$ forms a covalent $\sigma$ bond between the metal d $\sigma$ orbital and the $2\pi^*$ orbital on NO with delocalization of the N 2s orbital toward the metal whereas in the $^1\Sigma^+$ state, $PdNO^+$ forms a covalent $\pi$ bond with the metal d $\pi$ and NO $2\pi^*$ orbitals with $\sigma$ donation from NO to the metal. Apparently the GVB calculation does not describe the relative importance of these two bonding interactions for platinum as accurately as DFT.

The bonding in the charged and neutral group IB mononitrosyls remains essentially the same moving down the row. $CuNO^+$, $AgNO^+$, and $AuNO^+$ each have a one electron dative bond from the nitrosyl to the metal cation, decreasing the positive charge. The bonding analyses show that this orbital is composed predominantly of the in-plane NO($2\pi^*$) orbital, but that the metal contribution becomes more important moving down the row, i.e., 12% Cu, 15% Ag, and 34% Au.[15,86,87] In each case, the metal valence d orbitals are highly localized on the metal cation and do not participate significantly in the metal−nitrosyl bonding. However, the NBO analysis for $AuNO^+$ shows that the 5d orbitals account for 14% of the gold contribution to the dative bond, compared with 1% for the 4d orbitals in $AgNO^+$. This greater sd hybrid-

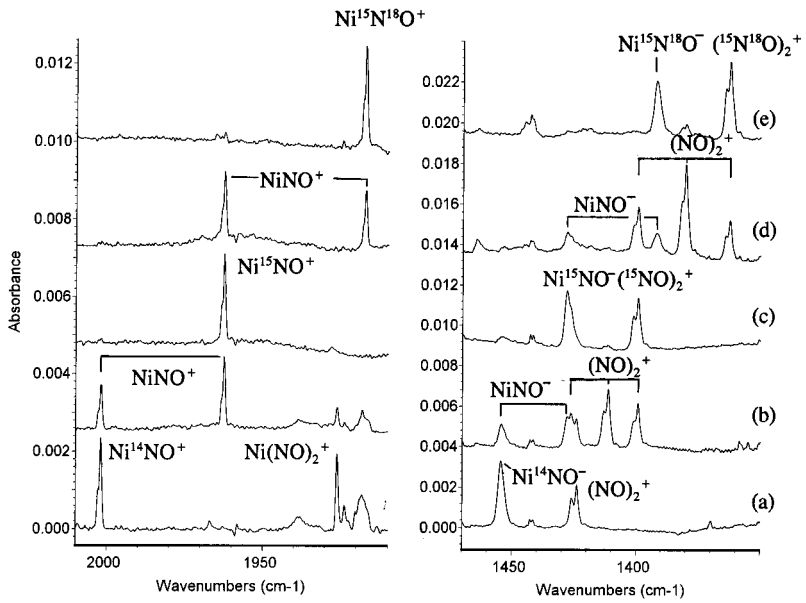


**Figure 14.** Infrared spectra in the 2010−1910 and 1470−1350 $cm^{-1}$ regions from co-deposition of laser-ablated nickel with isotopic NO in excess neon at 4 K: (a) 0.1% $^{14}N^{16}O$, (b) 0.1% $^{14}N^{16}O$ + 0.1% $^{15}N^{16}O$, (c) 0.1% $^{15}N^{16}O$, (d) 0.1% $^{15}N^{16}O$ + $^{15}N^{18}O$, and (e) 0.1% $^{15}N^{18}O$.

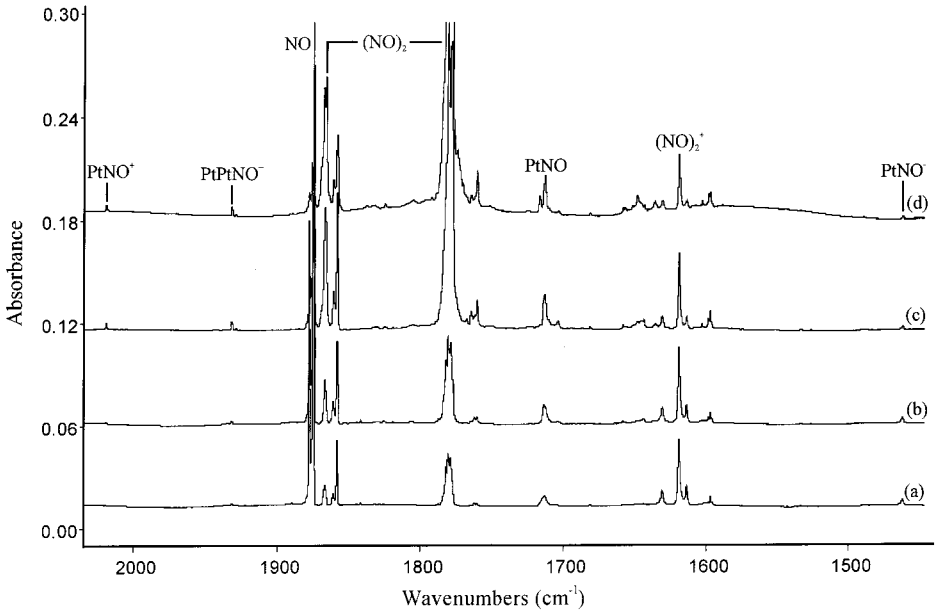


**Figure 15.** Infrared spectra in the 2030−1450 $cm^{-1}$ region for laser-ablated platinum co-deposited with 0.2% NO in Ne: (a) after 50 min deposition at 5 K, (b) after annealing to 8 K, (c) after annealing to 10 K, and (d) after annealing to 12 K.

ization on gold is probably due to the smaller s−d orbital energy difference in gold that arises from the relativistic contraction of the s levels and expansion of the d levels. Finally, Goldman and Krogh-Jesperson have pointed out that electrostatic effects increase the C−O force constant in $MCO^+$ cations,[96] and this effect contributes as well in the $MNO^+$ cations as all of their N−O fundamentals are above the NO value (1874.4 $cm^{-1}$ in solid neon).

The molecular orbitals for CuNO, AgNO, and AuNO are similar to those in the cations except that the uppermost orbital is now doubly occupied, and the metal atom makes a significantly greater contribution to the orbital than in the cations. This increases the M−N bonding character but weakens the N−O bond, as is apparent from the stretching frequencies and calculated bond lengths in the neutral mononitrosyls relative to the cations. The metal bonding is largely through the *n*s orbital; the (*n* − 1)d levels are again localized on the metal atom. The charges calculated for CuNO, AgNO, and AuNO species are summarized in Table 3. The natural charges on the metal decrease from +0.25 to +0.15 to +0.04 for CuNO, AgNO, and AuNO as the neon matrix frequency increases from 1602.2 to 1707.3 to 1710.4 $cm^{-1}$. The neon−argon matrix differences are 15.1, 27.3, and 8.5 $cm^{-1}$, respectively. While these differences for CuNO and AuNO are typical, the difference for AgNO is larger: this suggests that the more polarizable argon matrix is sustaining relatively more charge transfer from Ag to NO for AgNO in solid argon than solid neon.

**Table 3. Charges Calculated for $CuNO^{+,0}$, $AgNO^{+,0,-}$, and $AuNO^{+,0}$ Using the BPW91 and B3LYP Functionals[a]**

| molecule (ground state) | BPW91 Mulliken charges [spin density] natural charges | | | B3LYP Mulliken charges [spin density] natural charges | | |
|---|---|---|---|---|---|---|
| | $q_M$ | $q_N$ | $q_O$ | $q_M$ | $q_N$ | $q_O$ |
| $CuNO^+$ | +0.74 | −0.01 | +0.27 | +0.73 | +0.04 | +0.22 |
| ($^2A'$) | [0.17] | [0.51] | [0.32] | [0.11] | [0.54] | [0.35] |
| | +0.90 | +0.06 | +0.03 | +0.92 | +0.07 | +0.01 |
| CuNO | +0.18 | −0.31 | +0.13 | +0.16 | −0.25 | +0.09 |
| ($^1A'$) | +0.25 | −0.04 | −0.21 | +0.27 | −0.04 | −0.24 |
| $AgNO^+$ | +0.73 | −0.06 | +0.32 | +0.77 | −0.03 | +0.26 |
| ($^2A'$) | [0.20] | [0.51] | [0.29] | [0.15] | [0.54] | [0.31] |
| | +0.82 | +0.16 | +0.02 | +0.87 | +0.15 | −0.02 |
| AgNO | +0.11 | −0.30 | +0.19 | +0.11 | −0.25 | +0.14 |
| ($^1A'$) | +0.15 | +0.03 | −0.18 | +0.19 | +0.03 | −0.22 |
| $AgNO^-$ | −0.60 | −0.34 | −0.06 | −0.60 | −0.29 | −0.11 |
| ($^2A''$) | [−0.30] | [0.90] | [0.40] | [−0.48] | [1.03] | [0.46] |
| | −0.40 | −0.19 | −0.41 | −0.40 | −0.17 | −0.43 |
| $AuNO^+$ | +0.47 | +0.23 | +0.30 | +0.49 | +0.24 | +0.27 |
| ($^2A'$) | [0.57] | [0.18] | [0.25] | [0.46] | [0.24] | [0.30] |
| | +0.74 | +0.20 | +0.07 | +0.75 | +0.21 | +0.04 |
| AuNO | −0.24 | +0.08 | +0.16 | −0.19 | +0.06 | +0.13 |
| ($^1A'$) | +0.04 | +0.10 | −0.14 | +0.05 | +0.12 | −0.17 |

[a] References 84, 85, 86.

## C. Early TM Nitrosyl Anions

Figure 4B shows new bands at 1548.9, 1511.5, and 1463.1 $cm^{-1}$ that reveal mixed isotopic multiplets for three, one, and two NO subunits, respectively. The latter two bands were extremely photosensitive. BP86 calculations predicted a 118 $cm^{-1}$ red shift for $^3\Sigma^-$ $CrNO^-$ relative to CrNO, and the 1511.5 $cm^{-1}$ band down 103 $cm^{-1}$ from CrNO was assigned accordingly. Similar BP86 calculations predict a $^2A_1$ $Cr(NO)_2^-$ species with very strong 1483.3 $cm^{-1}$ antisymmetric stretching fundamental, and the 1463.1 $cm^{-1}$ band was likewise assigned.[26] These anion ground states are 26.3 and 45.3 kcal/mol below the neutral complexes at the BP86 level of theory, which provides estimates of chromium nitrosyl electron affinities.

The 1548.9 $cm^{-1}$ band is slightly increased by broadband photolysis, which destroys the absorptions assigned to $CrNO^-$ and $Cr(NO)_2^-$. This band shows a well-defined 2:1:1:2 quartet with isotopic mixtures, like that for a doubly degenerate mode,[58] and is in the position expected for $Cr(NO)_3^-$ anion, which should have a higher detachment energy than

$Cr(NO)_2^-$ and $CrNO^-$; the photodetachment of $CrNO^-$ and $Cr(NO)_2^-$ with growth of $Cr(NO)_3^-$ requires this relationship. Accordingly, the 1548.9 $cm^{-1}$ absorption was assigned by Zhou and Andrews[26] to $Cr(NO)_3^-$. With the expected nearly linear CrNO linkages, $Cr(NO)_3^-$ is a stable 16-electron anion. Note the absence of another band in this progression for a higher nitrosyl anion since $Cr(NO)_4$ is a closed shell species.

Our very recent DFT calculation[66] for $Cr(NO)_3^-$ found a $^1A_1$ ground state of $C_{3v}$ symmetry and a very strong doubly degenerate N−O stretching mode at 1563.1 $cm^{-1}$, in excellent agreement with the observed value. Furthermore, the energy is 61.2 kcal/mol lower than that for $Cr(NO)_3$, a higher electron affinity than predicted above for $Cr(NO)_2$, as suggested by the matrix photochemistry.[26]

## D. Late TM Nitrosyl Anions

The $MNO^-$ anions have been observed for five late transition metals. The $NiNO^-$ absorption at 1454.7 $cm^{-1}$ is illustrated in Figure 14, which again shows the isotopic behavior for a single NO vibration. In the anion cases, $CCl_4$ doping reduced the band to <10% of former yield, owing to the preferential capture of ablated electrons by $CCl_4$.

The series $NiNO^-$, $PdNO^-$, $PtNO^-$ was observed at 1454.7, 1487.6, 1462.1 $cm^{-1}$ in solid neon.[67,79] Common BPW91/6-311+G(d))/LANL2DZ calculations predicted strong 1454.4, 1499.6, and 1471.7 $cm^{-1}$ nitrosyl fundamentals for the $^1A'$ anion states, which is in excellent agreement and substantiates the assignments. Again the $^{14}N^{16}O/^{15}N^{16}O$ and $^{15}N^{16}O/^{15}N^{18}O$ isotopic frequency ratios (1.01910 and 1.02588 for $PtNO^-$) demonstrate evidence of coupling between the Pt−N and N−O stretching modes. Finally, the Pt−N stretching mode is calculated to be higher in $PtNO^-$ (BPW91, 674.5 $cm^{-1}$) than in PtNO (610.6 $cm^{-1}$) and $PtNO^+$ (568.5 $cm^{-1}$) as the extra electron contributes to the covalent $\sigma$ bond between Pt and NO.

The only anion observed in the copper family series is $AgNO^-$, and the bonding analyses show that the additional electron resides in an out-of-plane $\pi^*$ orbital almost completely localized on NO. Accordingly, the nitrosyl stretching frequency for $AgNO^-$ (1399.2 $cm^{-1}$) is significantly lower than that for AgNO and slightly higher than the experimental value for $NO^-$ (1352 $cm^{-1}$),[97] as expected from this description of the bonding. In this regard, alkali metals react with NO to produce ionic complexes, and alkaline earth and aluminum family metals form MNO complexes with varying degrees of charge transfer.[97−100] Aluminum is the only naked metal atom with clearly documented nitrosyl and isonitrosyl forms.[99]

Figure 16 contrasts neon matrix frequencies for the Fe−Co−Ni triad cation−neutral−anion species with BP86/6-311+G(d)/Wachters-Hay frequency calculations. The calculations give frequencies that are 40−60 $cm^{-1}$ too high, which shows very good predictive power. The cations are 131, 163, and 322 $cm^{-1}$ higher than the neutrals, and the anions are 208 and 225 $cm^{-1}$ lower; similar relationships have been observed for the Pd and Pt nitrosyls and for TM carbonyl species.[93] The large frequency jump from NiNO to $NiNO^+$ is augmented by the bent-linear structural change on ionization.

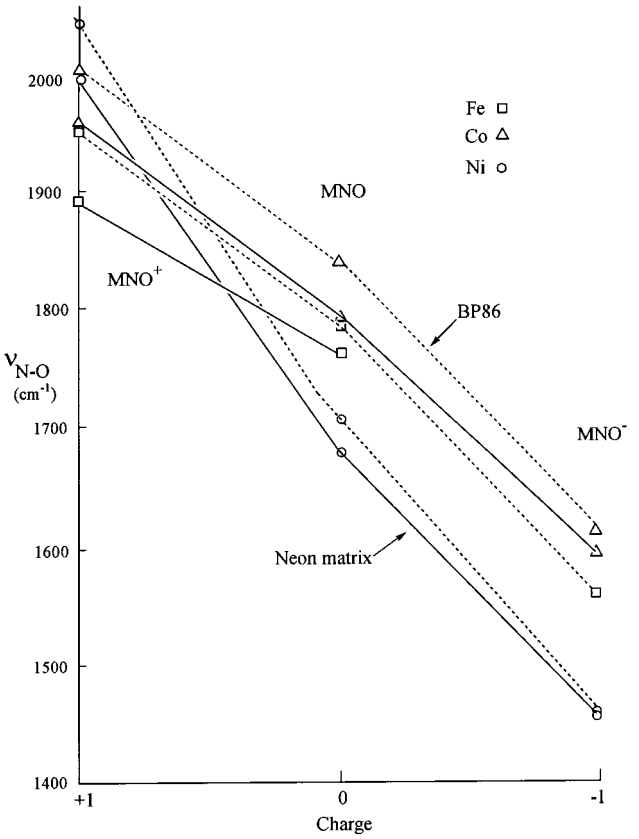


**Figure 16.** Plot of BP86/6-311+G*/modified Wachters−Hay calculated and neon matrix observed frequencies for Fe, Co, and Ni nitrosyl cations, neutrals, and anions.

Figure 17 compares the observed and calculated nitrosyl frequencies for $AgNO^{+,0,-}$ species using two matrix hosts and two density functionals.[80] Note that the neon matrix frequencies are higher than argon, by 6.6, 27.3, and 6.9 $cm^{-1}$, for the cation, neutral, and anion, respectively. The calculated BPW91 frequencies (6-311+G(d)/LANL2DZ) are +15.2, −40.5, and +75.0 $cm^{-1}$ (relative to neon matrix values); the AgNO result is an exception to the normal relationship and suggests that the pure density functional may be inadequate for AgNO. The calculated B3LYP frequencies are all high, as expected (91.1, 49.4, and 93.9 $cm^{-1}$ above neon matrix values). Note the marked difference between the charged and neutral species: the cation is higher by 199.1 $cm^{-1}$ and the anion lower by 312.6 $cm^{-1}$ than the neutral nitrosyl AgNO in solid neon.

## *V. Nitride-Oxide Insertion Products*

The nitride-oxide insertion products were independently discovered by Kushto et al. and Krim et al. in systematic investigations of TM reactions with NO.[59,60] The novel NTiO molecule was identified from Ti, N, and O isotopic shifts on the two bond-stretching modes, as described in section III.B, and from BP86 frequency calculations for the ground $^2A'$ state. The rate of the TM + NO insertion reaction and the

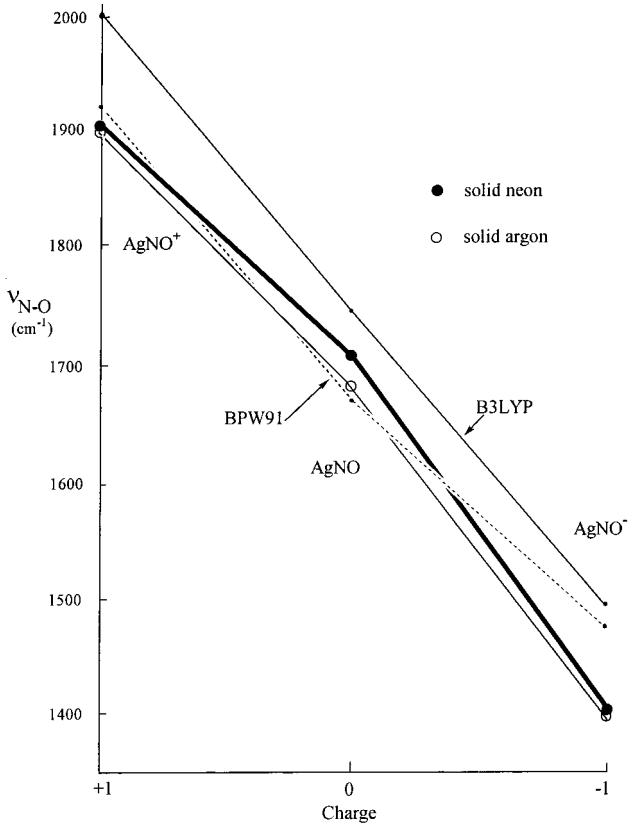


**Figure 17.** Plot of B3LYP and BP86/6-311+G*/LANL2DZ calculated and neon matrix observed N−O frequencies for $AgNO^{+,0,-}$ species.

relative yield of NMO insertion and MNO (or M[NO]) addition products varies across the periodic table. In the case of titanium discussed above, only the NTiO insertion product was formed, and this in large yield, but no insertion product was observed for the Ni group or Co, and the possible detection of NFeO is tentative.[67] Some of the NMO products grow during annealing the matrix, which indicates a spontaneous reaction while others require excitation from laser ablation or subsequent irradiation, which provides the activation energy required for the insertion reaction. This reaction behavior is summarized in Figure 18, which indicates NMO growth on annealing (∧) and on photolysis (*).

Bonding in the NMO molecules is revealed by the M−N and M−O stretching frequencies as assigned on the basis of isotopic shifts. These are relatively uncoupled bond stretching modes as the nitrogen and oxygen isotopic shifts are greater than or equal to about 90% of the isolated diatomic molecule values. Force constants for these two stretching modes calculated from argon matrix data[74] are given in Figure 18. Since five metal valence electrons are needed to form true nitride and oxide on the same metal center, it is logical that the M−N and M−O force constants increase to V and decrease thereafter on the first row as additional electrons become antibonding. Also note that the Sc−O and Ti−O stretching modes are higher than the Sc−N and Ti−N stretching modes, but with more metal valence electrons, the V−N and Cr−N modes are higher than the V−O and Cr−O modes (Table 1). The calculated

| | | | | | | | | | | | | | | | | | |
|---|---|---|---|---|---|---|---|---|---|---|---|---|---|---|---|---|---|
| Sc | * ∧ | | Ti | ∧ | | V | ∧ | | Cr | * | | Mn | * | | Fe | * | | Co | |
| | 149 | | | 353 | | | 649 | | | 619 | | | 553 | | | | | | |
| | 571 | | | 564 | | | 614 | | | 548 | | | 588 | | | | | | |
| Y | | | Zr | ∧ | | Nb | ∧ | | Mo | ∧ | | Tc | | | Ru | * | | Rh | |
| | | | | 347 | | | 670 | | | 707 | | | | | | 711 | | | 675 |
| | | | | 553 | | | 607 | | | 604 | | | | | | 547 | | | 541 |
| La | | | Hf | ∧ | | Ta | ∧ | | W | ∧ | | Re | ∧ | | Os | * ∧ | | Ir | |
| | | | | 379 | | | 697 | | | 774 | | | 839 | | | 849 | | | 720 |
| | | | | 614 | | | 662 | | | 737 | | | 722 | | | 710 | | | 656 |

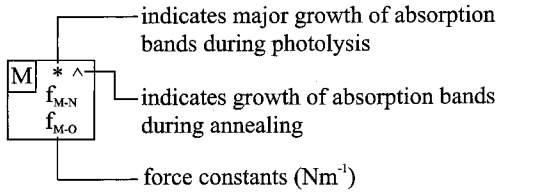


**Figure 18.** Mechanism of formation and force constants calculated for argon matrix-isolated NMO molecules.

bond lengths shown in Table 4 also reflect this trend. The force constant maximum is found for Mo in the second row, and there is a tie between Re and Os on the third row.

The NMnO insertion product is unique in that it is the only NMO molecule yet observed with extensively mixed M−N, M−O stretching modes, which are only 58 $cm^{-1}$ apart, and this mode mixing is not accounted for by the BP86 calculation for the $^3A''$ state.[27] Apparently, other low-lying d orbital configurations mix with the computed $^3A''$ state and make the NMnO ground state a difficult theoretical problem.

It is also useful to compare the force constants in NOsO and NRuO with those for the dioxides and dinitrides of these metals,[74,101−103] which are listed in Table 5. The M−N force constant (and presumably bond) in NMO is much stronger than in NMN, and the M−O force constant (and presumably bond) is weakened by a comparable amount relative to OMO. This can be explained by the smaller energy difference and greater interaction between the metal and nitrogen valence orbitals, strengthening the interaction between the metal and nitrogen at the expense of the metal−oxygen bond, which is manifested in NMO but not NMN and OMO where the nonmetal orbitals are the same. A like comparison with Cr, Mo, and W shows that these NMO molecules are true nitride *and* oxide with bonding comparable to the pure dioxide and dinitride molecules.[26,69] Finally, note that the third-row NMO force constants are all higher than their second-row counterparts. This increased bonding strength is probably due to the effect of relativistic bond-length contraction for the third-row metals.[63]

There is some correlation between the tendency to form NMO molecules and the metal surface to dissociate NO. Generally the higher melting point metals have a higher propensity to dissociate NO.[1] The lanthanide metals are an exception: all formed NLnO molecules[104] whereas the Ln metal melting points are all below the melting point of Pt, which did not form the insertion product.

The insertion reaction also proceeds with $(NO)_2$, as observation of $OTi(N_2)O$ and $OV(N_2)O$ indicate.[59,64] Vanadium shares with titanium this more extensive

**Table 4. Comparison of Ground State MNO Isomers Observed in Solid Argon and Parameters Calculated at the BP86 Level of Theory for First-Row TM Nitrosyls[a]**

| Sc[NO] | NTiO | NVO | NCrO | NMnO | FeNO | CoNO | NiNO | CuNO |
|---|---|---|---|---|---|---|---|---|
| $^1A'$ | $^2A'$ | $^1A'$ | $^2A''$ | $^3A''$ | $^2\Delta$ | $^1\Sigma^+$ | $^2A'$ | $^1A'$ |
| 1.814[b] | 1.715[b] | 1.571 | 1.547 | 1.550 | 1.593[b] | 1.569 | 1.665 | 1.901 |
| 1.840[c] | 1.661[c] | 1.632 | 1.624 | 1.619 | 1.186[b] | 1.182 | 1.187 | 1.185 |
| 1.524[d] | 105.8°[e] | 107.8° | 114.4° | 117.0° | 180°[e] | 180° | 140.2° | 120.3° |
| NScO | | V[NO] | CrNO | MnNO | Fe[NO] | Co[NO] | $^2$Ni[NO] | |
| $^3A''$ | | $^2A''$ | $^4\Sigma^-$ | $^3\Sigma^-$ | $^2A''$ | $^1A'$ | $A''$ | |
| (+8.5)[f] | | (+20.5) | (+5.6) | (+7.1) | (+20.4) | (+16.8) | (+20.5) | |
| 2.112[b] | | 1.711[b] | 1.667[b] | 1.637 | 1.703 | 1.669 | 1.783 | |
| 1.699[c] | | 1.831[c] | 1.212[d] | 1.190 | 1.964 | 1.906 | 1.891 | |
| 112.7°[e] | | 1.392[d] | 180° | 180° | 1.268 | 1.253 | 1.271 | |
| ScNO | | VNO | Cr[NO] | Mn[NO] | | | | |
| $^3\Pi$ | | $^3\Delta$ | $^4A''$ | $^3A''$ | | | | |
| (+9.8)[f] | | (+41.0) | (+16.4) | (+19.8) | | | | |
| 1.856[b] | | 1.677 | 1.760[b] | 1.752 | | | | |
| 1.230[d] | | 1.215 | 1.859[c] | 1.951 | | | | |
| 180°[e] | | 180° | 1.343[d] | 1.275 | | | | |

[a] Basis sets 6-31+G* for N and O, Wachters for Sc and Ti, and 6-311+G* and all-electron set of Wachters−Hay for all other calculations—refs 59, 64, 26, 27, 67, and 84. [b] Metal−N distance, Å. [c] Metal−O distance, Å. [d] N−O distance, Å. [e] Bond angle, deg. [f] Energy above global minimum, kcal/mol.

**Table 5. Comparison of Force Constants (N m$^{-1}$) Calculated for NMN, OMO, and NMO (M = Os, Ru)**

| | | osmium | | ruthenium | |
|---|---|---|---|---|---|
| molecule | bond | $f_{M-X}$ | $f_{M-X/M-Y}$ | $f_{M-X}$ | $f_{M-X/M-Y}$ |
| NMN | M−N | 722 | 115 | 588 | 115 |
| NMO | M−N | 849 | 79 | 711 | 110 |
| | M−O | 710 | | 547 | |
| OMO | M−O | 828 | 72 | 694[a] | 99[a] |

[a] From ref 101.

reaction with $(NO)_2$, owing to the great stability of vanadium and titanium oxide bonds.

## *VI. Nitrosyls on Transition Metal Surfaces and Cations in Catalyst Systems*

The spectra of MNO and $MNO^+$ species provide simple models for NO chemisorbed on metal surfaces[1] and in contact with metal cations in zeolite catalyst systems.[3] As listed in Tables 1 and 2 and shown in Figures 16 and 17, adding electrons to $MNO^+$ to form MNO and $MNO^-$ decreases the nitrosyl vibrational frequencies, and Mulliken and natural charge distributions show an increase in negative charge on the NO submolecule.

The chemistry of group VIII metals and their interaction with nitric oxide has been investigated extensively on zeolites and metal oxides where NO is a probe for assessing the state of the active metallic species.[105−112] Unfortunately, assignments to specific nitrosyls are not straightforward, and the matrix spectroscopy can help in this regard. Iron(II) zeolite spectra are characterized by a dominant band near 1880 cm$^{-1}$, which appears immediately after exposure to low NO pressure and has been ascribed to a mononitrosyl species, and weaker bands near 1910 and 1810 cm$^{-1}$, which increase with more NO and have been identified first as dinitrosyl[106,107,110] and finally as trinitrosyl[108] on the basis of mixed $^{14}$NO/$^{15}$NO isotopic spectra. The $FeNO^{2+}$, $FeNO^+$, and FeNO mononitrosyl frequencies are calculated as

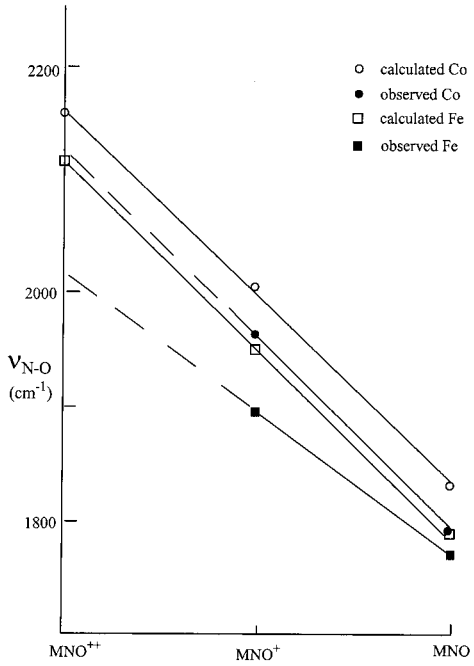


**Figure 19.** Plot of BP86/6-311+G*/modified Wachters−Hay calculated and neon matrix observed frequencies for $CoNO^{2+}$, $CoNO^+$, CoNO and $FeNO^{2+}$, $FeNO^+$, FeNO.

2123.0, 1951.0, and 1785.7 cm$^{-1}$ at the BP86 level. The present scale factor for $FeNO^+$ predicts isolated $FeNO^{2+}$ at 2064 cm$^{-1}$ to go with the observed $FeNO^+$ and FeNO at 1897 and 1766 cm$^{-1}$ in solid neon.[67] Comparison with this scale and Figure 19 shows that the 1880 cm$^{-1}$ absorbing mononitrosyl species involves iron cation with a local charge near +1 *but certainly not* +2. For ferrous cations on metal oxides, mononitrosyls absorbing near 1810 and 1750 cm$^{-1}$ have been observed.[107,109] Clearly, the 1810 cm$^{-1}$ absorption is due to an iron nitrosyl with *only a partial* positive charge, and the 1750 cm$^{-1}$ band is due to a reduced nearly neutral iron nitrosyl species.

Infrared spectra of cobalt(II) zeolites exposed to NO exhibit bands close to 1900 and 1815 cm$^{-1}$, and a

band at 1880 $cm^{-1}$ in the $Co^{II}X$ system has been assigned to the mononitrosyl complex of this ion.[105] These frequencies are intermediate between those observed for the neutral and +1 cation Co(NO) and $Co(NO)_2$ species in solid neon and allow an estimate of the charge at the active cobalt center to be made.[67] Plots of the NO frequency vs charge for both $Co(NO)^{+,0,-}$ (Figure 16) and $Co(NO)_2^{+,0,-}$ show linear relationships. The $^3\Delta$ state $CoNO^{2+}$ species is calculated at 2160 $cm^{-1}$, higher by 150 $cm^{-1}$ than $CoNO^+$. The 1880 and 1815 $cm^{-1}$ mononitrosyl and dinitrosyl absorptions quoted above yield effective charges of +0.4 and +0.5, respectively, at the cobalt centers. Finally, $Ni^{2+}$ zeolites gave a strong nitrosyl band at 1892 $cm^{-1}$, which was interpreted as $(Ni^+)(NO^+)$.[112] In the neon matrix experiments, $NiNO^+$ at 2001.9 $cm^{-1}$ and NiNO at 1680.1 $cm^{-1}$ clearly bracket the 1892 $cm^{-1}$ Ni(NO)/zeolite absorption and suggest that the local charge is near +0.7 at the metal site.

It is generally accepted that Cu-exchanged zeolites contain a mixture of $Cu^+$ and $Cu^{2+}$ ions, coordinated to the zeolite lattice and charge compensated by anionic Al T-sites.[3] Both $Cu^+$ and $Cu^{2+}$ sites adsorb single NO molecules. The N−O stretching frequency for Cu(I)-NO/zeolite is reported near 1800 $cm^{-1}$ depending on the zeolite,[3,113] which is about 2/3 of the way between the neon matrix CuNO and $CuNO^+$ frequencies, and a +0.7 net charge on the CuNO center is estimated. An average Cu(II)-NO/zeolite frequency[113] at 1900 $cm^{-1}$ is near the neon matrix $CuNO^+$ frequency,[84] which suggests a +1.0 net charge on the CuNO center for this *formally* Cu(II) NO/zeolite species.

Copper cation sites in zeolite also bind two NO molecules to form Cu-gem-dinitrosyl species, which have been suggested to play an important role in NO decomposition.[3,113,114] This dinitrosyl species is bent, with comparable intensities for symmetric and antisymmetric N−O vibrations observed at 1824 and 1727−1738 $cm^{-1}$ in Cu−ZSM. The $Cu(NO)_2$ species observed in matrix-isolation experiments is linear; however, DFT calculations predict that both bent $Cu(NO)_2^+$ and $Cu(NO)_2$ are stable.[84] The symmetric and antisymmetric N−O stretching vibrations of the bent $^1A_1$ state $Cu(NO)_2^+$ are 2−4% lower than for the linear $^3\Sigma_g^-$ state $Cu(NO)_2^+$, and the $^2B_1$ state $Cu(NO)_2$ frequencies are 6−9% lower than for the $^2\Pi_u$ state $Cu(NO)_2$. If the calculated frequencies for bent $Cu(NO)_2$ and $Cu(NO)_2^+$ are scaled by the factor 0.94 from the matrix-isolated linear dinitrosyl species, the Cu-gem-dinitrosyl frequencies are approximately equal to the scaled 1789 and 1731 $cm^{-1}$ values for bent $Cu(NO)_2^+$. Therefore, Zhou and Andrews concluded that the net charge on Cu-gem-dinitrosyl is approximately +1. In like fashion, charges have been estimated for Rh(I)CO and $Rh(I)(CO)_2$ on zeolites from RhCO and $Rh(CO)_2$ spectra in solid neon and DFT calculations.[115]

The MNO nitrosyl frequencies are very good models for NO adsorbed to a single TM atom in top sites on metal surfaces in some cases and very poor in others as a comparison of Table 1 here and in ref 1 demonstrates. Nickel and copper bracket the range of agreement: the neon matrix NiNO fundamental is 1680.1 $cm^{-1}$ and the top site frequency (also called on-top and atop) on Ni(111) is 1681 $cm^{-1}$ whereas CuNO absorbs at 1602.2 $cm^{-1}$ in solid neon and at 1823 $cm^{-1}$ on Cu(111).[67,84,116,117] The latter probably reflects a structural difference, which clearly affects the bonding based on structure-bonding relationships revealed by theoretical calculations.[14,44] Silver is equally unclear: absorptions at 1839 and 1710 $cm^{-1}$ have been ascribed to linear and bent atop site AgNO.[117] The latter is near the isolated (bent) AgNO complex 1707 $cm^{-1}$ absorption.[85]

The adsorption of nitric oxide on nickel group metal surfaces is predominantly molecular in nature, and molecules in both bridged and on-top sites have been reported.[1] On the Pt(110) surface, bands are observed at 1610−1630 $cm^{-1}$ and assigned to 2-fold bridge sites.[118] At high coverage, the bridged species disappears and is replaced by an on-top species with a 1760 $cm^{-1}$ frequency. The difference between these frequencies, 130−150 $cm^{-1}$, is comparable to the 155 $cm^{-1}$ difference between PtNO and $(Pt_2)NO$ observed in solid argon.[79]

Similar results are found for NO on Pd(111), where bands observed at 1734−1758 $cm^{-1}$ and 1586−1620 $cm^{-1}$ are assigned to NO at top and 2-fold bridge sites, the frequencies depending on the coverage.[119] The results of DFT calculations for NO chemisorbed on palladium clusters indicate that the molecule is perpendicular to the surface.[120] The difference of 140−150 $cm^{-1}$ between these sites is comparable to the 157 $cm^{-1}$ difference between PdNO and $(Pd_2)NO$ observed in solid argon. This indicates that results for NO bound to one and two metal atoms can reproduce the frequency differences observed for different adsorption sites on the respective metal surfaces. On Ni(100), bands of increasing frequency in the range 1300−1700 $cm^{-1}$ are observed as the coverage is increased and attributed to NO bound to progressively lower coordination sites.[121] The bridge frequency range (1475−1513 $cm^{-1}$) brackets the 1504 $cm^{-1}$ absorption for $(Ni_2)NO$ in the matrix,[79] and the top site agreement is ±1 $cm^{-1}$.

When NO is adsorbed on Ir(111) at sufficiently high coverage, a band is observed at 1860 $cm^{-1}$ that is most likely due to NO in a top site,[122] with an analogous band observed near 1840 $cm^{-1}$ on Ir(100).[123] These are very close to the 1851.1 and 1835.8 $cm^{-1}$ values observed for IrNO isolated in solid neon and argon.[75] Good agreement is also found between the vibrational data for matrix-isolated and surface rhodium nitrosyls. Nitric oxide absorbs at 1830 $cm^{-1}$ on top sites of Rh(111) at sufficiently high coverages.[124,125] This is quite close to the 1806.4 $cm^{-1}$ band for RhNO in neon.[75] The match for cobalt is not quite as good,[1,67] and this may arise from a CoNO structural difference.

## VII. Summary

Transition metal atoms react with nitric oxide to form the simple end-bonded and side-bonded nitrosyls and the novel nitride-oxide insertion product. The relative yield of these primary products depends on the strengths of the metal nitride and metal oxide bonds. For titanium, only NTiO is observed; but for copper, only CuNO is formed. Table 4 summarizes

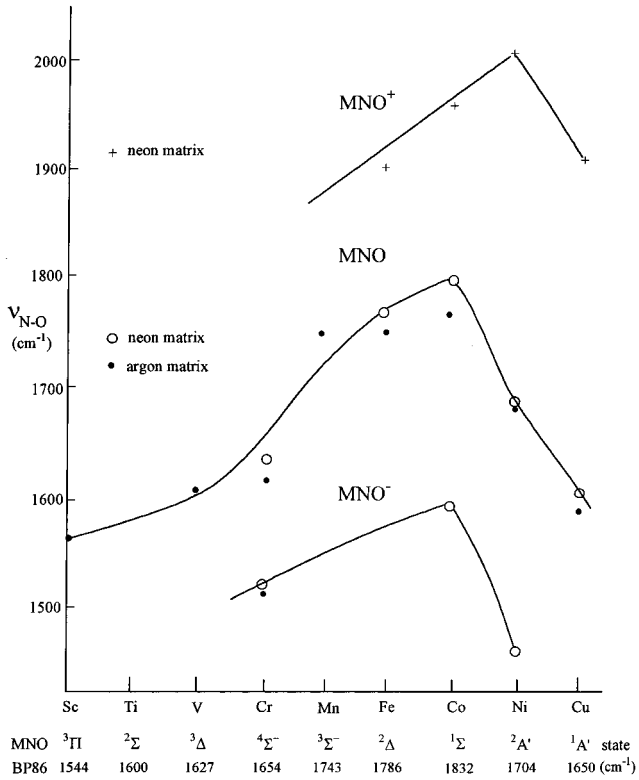


**Figure 20.** Plot of observed first-row $MNO^+$, MNO, and $MNO^-$ frequencies. BP86 calculated MNO states and N−O stretching frequencies are listed below.

the relative energies and electronic states for all observed first-row MNO product isomers calculated at the BP86 level. The noble gas matrix provides a good medium to investigate the stable NMO insertion products, which may require collisional deactivation to survive the highly exothermic insertion reaction, and the metastable side-bound M[NO] isomers formed by irradiation of end-bound MNO nitrosyls. The Fe, Co, and Ni nitrosyls undergo $\eta^1$ to $\eta^2$ photoisomerism. Annealing to allow diffusion and reaction of more NO facilitates the spontaneous formation of higher nitrosyls, $M(NO)_x$, which are identified from multiplet infrared absorptions in mixed isotopic spectra.

Laser ablation provides TM cations, atoms, and electrons for reactions, and the N−O stretching frequencies for $MNO^+ > MNO > MNO^-$ exhibit large diagnostic separations, which is consistent with the magnitude of the metal d to NO $2\pi^*$ donation. This is illustrated for silver in Figures 13 and 17. The experimental frequency data for first-row nitrosyls are plotted in Figure 20; the corresponding BP86 calculated states and frequencies are shown below. For a given charge, a general increase in N−O stretching frequency is found with increasing metal atomic number for MNO species to a maximum at cobalt for linear structures of neutral and anion and at nickel for cation complexes. Similar trends are found in the systematic calculations of frequencies for MNO and $MNO^+$ species.[14,15] This increase in N−O frequency follows the decrease in metal to NO $2\pi^*$ donation with increasing metal ionization energy for linear structures, and the decrease in N−O frequencies accompanies a structural change from linear to bent. As discussed for $CuNO^+$, the nonbonding d-manifold is filled, and electrons must occupy $2\pi^*$ orbitals.[15] The bent NiNO and CuNO molecules are weakly bound complexes.[14]

The discussion involves neon and argon matrix frequencies, and it is useful to compare frequencies in both matrix hosts. The neon matrix frequencies are expected to be better predictions for future gas-phase investigations. As no gas-phase data are available for MNO species, we suggest the reaction of laser-ablated TM atoms with NO in a pulsed-nozzle expansion to form these interesting transient molecules for high-resolution spectroscopic investigation. The MNO frequencies in solid neon or argon also provide benchmarks for comparison of NO adsorbed on metal surfaces and NO ligands in larger TM complexes.

The bonding trends are described by DFT calculations of vibrational frequencies. Table 6 compares the observed and calculated frequencies for Fe, Co, Ni group nitrosyls using pure density functionals. For cation, neutral, and anion alike, most of the calculated frequencies are high by 1−2% as expected. Comparable scale factors have been reported for stable TM compounds.[43] The worst case is Fe[NO] where Fe−O and Fe−N bonds and several d orbital configurations are involved.[67,73] Even second- and third-row TM nitrosyls are modeled very well using a pseudopotential; however, the heavy metal−N bonds are less accurately described than the N−O bonds. In most cases we find that the BP86 functional predicts observed frequencies more accurately than B3LYP, in agreement with an earlier study,[43] and that the newer BPW91 functional gives nearly the same frequencies as BP86.[126]

Often DFT predicts two low-lying states, and the true ground state cannot be determined. However, if the calculated frequencies are clearly different for the two states, as is the case for CoNO and CuNO, the ground state will be the state whose frequencies are observed in the low-temperature solid matrix. For the CoNO example, the BP86 functional predicts the $^1\Sigma^+$ state lower than $^3A''$, but the B3LYP functional finds the reverse energy order. However, both functionals give frequencies for CoNO that are compatible with the observed matrix values only for $^1\Sigma^+$ as the ground state.[67] For the CuNO case, BP86 predicts the $^1A'$ ground state, which is confirmed by matching three calculated and observed argon matrix isotopic fundamentals.[44,84,85] However, for FeNO and NiNO, both functionals give consistent relative energies and agree on the ground states.[67] The bottom line here is that one density functional does not work best for everything; since the two functionals treat exchange and correlation differently, it is advisable to perform calculations with both pure and hybrid density functionals to compare with experimental observations.

Isotopic frequencies can be easily calculated, and the isotopic frequency ratios employed as a measure of the normal vibrational mode for comparison with observed values. The coupling between M−N and N−O stretching vibrations varies with the transition metal, the charge on the species, the number of NO molecules, and the geometry, and accordingly, the calculated and observed isotopic frequency ratios

**Table 6. Comparison of Observed (Neon and Argon) and Calculated Vibrational Frequencies ($cm^{-1}$) and Scale Factors (Neon/Calculated) for Group VIII Nitrosyl Species**

| molecule | obsd (Ne) | obsd (Ar) | calcd[a] | scale factor |
|---|---|---|---|---|
| $FeNO^+$ | 1897.3 | | 1951.0 | 0.972 |
| FeNO | 1766.0 | 1748.9 | 1785.7 | 0.989 |
| $Fe(NO)_2$ | 1810.8 | 1798.1 | 1825.6 | 0.992 |
| | 1744.6 | 1731.6 | 1752.4 | 0.996 |
| $Fe(NO)_3$ | 1757.8 | 1742.6 | 1775.0 | 0.990 |
| Fe-($\eta^2$-NO) | 1342.2 | 1343.8 | 1271.0 | 1.056 |
| $RuNO^+$ | 1918.0 | | 1955.0 | 0.981 |
| RuNO | 1785.8 | 1765.9 | 1804.3 | 0.990 |
| $Ru(NO)_2$ | 1805.3 | | 1802.5 | 1.002 |
| | 1721.4 | 1709.6 | 1735.4 | 0.992 |
| $Ru(NO)_3$ | 1741.1 | 1738.9 | 1743.0 | 0.999 |
| $OsNO^+$ | 1921.8 | 1901.5 | 1956.6 | 0.982 |
| OsNO | 1809.4 | 1789.1 | 1846.1 | 0.980 |
| $Os(NO)_2$ | | 1815.8 | 1817.6 | |
| | 1726.9 | 1717.9 | 1751.7 | 0.986 |
| $Os(NO)_3$ | 1753.2 | 1745.5 | 1757.2 | 0.998 |
| $CoNO^+$ | 1957.5 | | 2009.6 | 0.974 |
| CoNO | 1794.2 | 1761.0 | 1832.0 | 0.979 |
| $Co(NO)_2$ | 1749.1 | 1827.2 | 1836.7 | 0.990 |
| | | 1737.6 | 1767.3 | |
| $Co(NO)_3$ | 1825.6 | 1814.6 | 1886.2 | 0.968 |
| | 1782.1 | 1770.1 | 1796.0 | 0.992 |
| Co-($\eta^2$-NO) | 1317.4 | 1284.2 | 1341.8 | 0.982 |
| $CoNO^-$ | 1585.7 | | 1611.6 | 0.984 |
| $Co(NO)_2^-$ | 1593.8 | | 1598.0 | 0.997 |
| $RhNO^+$ | 1957.5 | | 1990.8 | 0.983 |
| RhNO | 1806.4 | 1775.1 | 1785.6 | 1.012 |
| $Rh(NO)_2$ | | 1801.8 | 1823.5 | |
| | 1746.9 | 1736.5 | 1764.0 | 0.990 |
| $Rh(NO)_3$ | 1757.7 | 1749.0 | 1779.9 | 0.988 |
| $IrNO^+$ | 1990.0 | | 2023.9 | 0.983 |
| IrNO | 1851.1 | 1833.7 | 1878.9 | 0.985 |
| $Ir(NO)_2$ | | 1742.2 | 1779.0 | |
| $Ir(NO)_3$ | 1753.7 | 1745.5 | 1781.0 | 0.985 |
| $NiNO^+$ | 2001.9 | | 2043.2 | 0.980 |
| NiNO | 1680.1 | 1676.6 | 1703.9 | 0.986 |
| $Ni(NO)_2$ | 1762.0 | 1749.7 | 1777.3 | 0.991 |
| Ni-($\eta^2$-NO) | 1292.6 | 1293.7 | 1313.4 | 0.984 |
| $NiNO^-$ | 1454.7 | | 1456.4 | 0.999 |
| $Ni(NO)_2^-$ | 1592.2 | | 1596.5 | 0.997 |
| $PdNO^+$ | 1924.0 | 1921.6 | 1967.9 | 0.978 |
| PdNO | 1676.4 | 1661.8 | 1700.1 | 0.986 |
| $Pd(NO)_2$ | 1753.0 | 1733.8 | 1774.7 | 0.988 |
| $PdNO^-$ | 1487.6 | | 1499.6 | 0.992 |
| $PtNO^+$ | 2019.6 | 2010.4 | 2043.8 | 0.988 |
| PtNO | 1712.6 | 1677.0 | 1717.6 | 0.997 |
| $Pt(NO)_2$ | (1780) | 1763.8 | 1794.3 | 0.992 |
| $PtNO^-$ | 1462.1 | | 1471.7 | 0.993 |

[a] BP86/6-311+G(d)/Wachters−Hay for first row and BPW91/6-311+G(d)/LANL2DZ for second and third rows.

provide another diagnostic for the new molecule or ion. Members of the $V(NO)_{1,2,3}$ series provide a good illustration of this point.[64]

Finally, the investigation of vibrational frequencies in unsaturated TM nitrosyl cations, neutrals, and anions clearly benefits from a close working relationship between experimental measurement and computational theory to identify and characterize a large number of important new molecular species.

## VIII. Acknowledgments

The authors gratefully acknowledge the assistance of B. Liang and X. Wang, unpublished results, useful discussions, and three figures from L. Manceron, helpful correspondence with E. Alikhani and C. W. Bauschlicher, Jr., and financial support from N.S.F. Grant CHE 00-78836.

## IX. References

(1) Brown, W. A.; King, D. A. *J. Phys. Chem. B* **2000**, *104*, 2578 and references therein.
(2) Schlögl, R. *Angew. Chem.* **1993**, *105*, 402.
(3) Shelef, M. *Chem. Rev.* **1995**, *95*, 209.
(4) (a) Zöllner, H.; Kraser, W.; Woike, T.; Haussühl, S. *Chem. Phys. Lett.* **1989**, *161*, 497. (b) Woike, Th.; Haussühl, S. *Solid State Commun.* **1993**, *86*, 333.
(5) Guida, J. A.; Aymonino, P. J.; Piro, O. E.; Castellano, E. E. *Spectrochim. Acta* **1993**, *49A*, 535. Guida, J. A.; Piro, O. E.; Aymonino, P. J. *Inorg. Chem.* **1995**, *34*, 4113.
(6) (a) Carducci, M. D.; Pressprich, M. R.; Coppens, P. *J. Am. Chem. Soc.* **1997**, *119*, 2669. (b) Coppens, P.; Fomitchev, D. V.; Carducci, M. D.; Culp, K. *J. Chem. Soc., Dalton Trans.* **1998**, 865.
(7) (a) Fromitchev, D. V.; Furlani, T. R.; Coppens, P. *Inorg. Chem.* **1998**, *37*, 1519. (b) Fomitchev, D. V.; Coppens, P.; Li, T.; Bagley, K. A.; Chen, L.; Richter-Addo, G. B. *Chem. Commun.* **1999**, 2013.
(8) Culotta, E.; Koshland, D. E., Jr. *Science* **1992**, *258*, 1862.
(9) Verma, A.; Hirsch, D. J.; Glatt, C. E.; Ronnett, G. V.; Snyder, S. H. *Science* **1993**, *259*, 381.
(10) Wink, D. A.; Grisham, M. B.; Mitchell, J. B.; Ford, P. C. *Methods in Enzymology*; Packer, L., Ed.; Academic Press: San Diego, 1996; Vol. 268.
(11) Cheng, L.; Richter-Addo, G. B. Binding and Activation of Nitric Oxide by Metalloporphyrins and Heme. *The Porphyrin Handbook*; Kadish, K. M., Smith, K. M., Guiland, R., Eds.; Academic Press: San Diego, 2000; Chapter 33, Vol. 4,
(12) Squadrito, G. L.; Pryor, W. A. *Free Radical Biol. Med.* **1998**, *25*, 392 and references therein.
(13) Enemark, J. H.; Feltham, R. D. *Coord. Chem. Rev.* **1974**, *13*, 339. Wescott, B. L.; Enemark, J. H. Transition Metal Nitrosyls. *Inorganic Electronic Structure and Spectroscopy*; Solomon, E. I., Lever, A. B. P., Eds.; John Wiley and Sons: New York, 1999; Chapter 7, Vol. 2,
(14) Blanchet, C.; Duarte, H. A.; Salahub, D. R. *J. Chem. Phys.* **1997**, 106, 8778.
(15) Thomas, J. L. C.; Bauschlicher, C. W., Jr.; Hall, M. B. *J. Phys. Chem.* A **1997**, 101, 8530.
(16) Hass, K. C.; Tsai, M.-H.; Kasowski, R. V. *Phys. Rev. B* **1996**, *53*, 44. Ge, Q.; Brown, W. A.; Sharma, R. K.; King, D. A. *J. Chem. Phys.* **1999**, *110*, 12082.
(17) Perutz, R. N.; Turner, J. J. *J. Am. Chem. Soc.* **1975**, *97*, 4800.
(18) Kundig, E. P.; McIntosh, D.; Moskovits, M.; Ozin, G. A. *J. Am. Chem. Soc.* **1973**, *95*, 7234.
(19) Joly, H. A.; Manceron, L. *Chem. Phys.* **1998**, *226*, 61.
(20) Zhou, M. F.; Chertihin, G. V.; Andrews, L. *J. Chem. Phys.* **1998**, *109*, 10893.
(21) Zhou, M. F.; Andrews, L. *J. Chem. Phys.* **1999**, *110*, 10370.
(22) Liang, B.; Zhou, M. F.; Andrews, L. *J. Phys. Chem. A* **2000**, *104*, 3905.
(23) Chiarelli, J. A.; Ball, D. W. *J. Phys. Chem.* **1994**, *98*, 12828.
(24) Ball, D. W.; Chiarelli, J. A. *J. Mol. Struct.* **1995**, *373*, 113.
(25) Ruschel, G. K.; Nemetz, T. M.; Ball, D. W. *J. Mol. Struct.* **1996**, *384*, 101.
(26) Zhou, M. F.; Andrews, L. *J. Phys. Chem. A* **1998**, *102*, 7452. The computed Cr−N−O angle is 169.8° (all cis) for $^3B_2$ $Cr(NO)_2$.
(27) Andrews, L.; Zhou, M. F.; Ball, D. W. *J. Phys. Chem. A* **1998**, *102*, 10041.
(28) Krim, L.; Manceron, L.; Alikhani, M. E. *J. Phys. Chem. A* **1999**, *103*, 2592.
(29) Satija, S. K.; Swanson, B. I.; Crichton, O.; Rest, A. J. *Inorg. Chem.* **1978**, *17*, 1737.
(30) Crichton, O.; Rest, A. J. *J. Chem. Soc., Dalton Trans.* **1977**, 202 and 208.
(31) Crichton, O.; Rest, A. J. *J. Chem. Soc., Dalton Trans.* **1977**, 656.
(32) Crichton, O.; Rest, A. J. *J. Chem. Soc., Dalton Trans.* **1977**, 536.
(33) Wang, X.; Zhou, M. F.; Andrews, L. *J. Phys. Chem. A* **2000**, *104*, 7964.
(34) Wang, X.; Zhou, M. F.; Andrews, L. *J. Phys. Chem. A* **2000**, *104*, 10104.
(35) Wang, X.; Andrews, L. *J. Phys. Chem. A* **2001**, *105*, 4403.
(36) Swanson, B. I.; Satija, S. K. *J. Chem. Soc. Chem. Commun.* **1973**, 40.
(37) Bondybey, V. E.; Smith, A. M.; Agreiter, J. *Chem. Rev.* **1996**, *96*, 2113.
(38) Burkholder, T. R.; Andrews, L. *J. Chem. Phys.* **1991**, *95*, 8697.
(39) Hassanzadeh, P.; Andrews, L. *J. Phys. Chem.* **1992**, *96*, 9177.
(40) Zhou, M. F.; Andrews, L. *J. Am. Chem. Soc.* **1998**, *120*, 11499.
(41) Zhou, M. F.; Andrews, L. *J. Am. Chem. Soc.* **1998**, *120*, 13230.
(42) Zhou, M. F.; Andrews, L. *J. Chem. Phys.* **1999**, *110*, 2414, 6820.
(43) Bytheway, I.; Wong, M. W. *Chem. Phys. Lett.* **1998**, *282*, 219.
(44) Hrušák, J.; Koch, W.; Schwarz, H. *J. Chem. Phys.* **1994**, *101*, 3898.
(45) Becke, A. D. *J. Chem. Phys.* **1993**, *98*, 5648.
(46) Stephens, P. J.; Devlin, F. J.; Chabalowski, C. F.; Frisch, M. J. *J. Phys. Chem.* **1994**, *98*, 11623.
(47) Becke, A. D. *Phys. Rev. A* **1988**, *38*, 3098.

(48) Perdew, J. P. *Phys. Rev. B* **1986**, *33*, 8822 and erratum *34*, 7406.
(49) Frisch, M. J.; Trucks, G. W.; Schlegel, H. B.; Scuseria, G. E.; Robb, M. A.; Cheeseman, J. R.; Zakrzewski, V. G.; Montgomery, J. A.; Jr.; Stratmann, R. E.; Burant, J. C.; Dapprich, S.; Millam, J. M.; Daniels, A. D.; Kudin, K. N.; Strain, M. C.; Farkas, O.; Tomasi, J.; Barone, V.; Cossi, M.; Cammi, R.; Mennucci, B.; Pomelli, C.; Adamo, C.; Clifford, S.; Ochterski, J.; Petersson, G. A.; Ayala, P. Y.; Cui, Q.; Morokuma, K.; Malick, D. K.; Rabuck, A. D.; Raghavachari, K.; Foresman, J. B.; Cioslowski, J.; Ortiz, J. V.; Baboul, A. G.; Stefanov, B. B.; Liu, G.; Liashenko, A.; Piskorz, P.; Komaromi, I.; Gomperts, R.; Martin, R. L.; Fox, D. J.; Keith, T.; Al-Laham, M. A.; Peng, C. Y.; Nanayakkara, A.; Gonzalez, C.; Challacombe, M.; Gill, P. M. W.; Johnson, B.; Chen, W.; Wong, M. W.; Andres, J. L.; Gonzalez, C.; Head-Gordon, M.; Replogle, E. S.; Pople, J. A. *Gaussian 98, Revision A.7*; Gaussian, Inc.: Pittsburgh, PA, 1998.
(50) Bauschlicher, C. W., Jr.; Ricca, A.; Partridge, H.; Langhoff, S. R. In *Recent Advances in Density Functional Theory*, Part II; Chong, D. P., Ed.; World Scientific Publishing: Singapore, 1997.
(51) In a special issue of *Chemical Reviews* on Computational Transition Metal Chemistry, an article on the nature of bonding in TM compounds (Frenking, G.; Frolich, N. *Chem. Rev.* **2000**, *100*, 717) described quantum chemical methods that can be applied to TM-NO complexes and discussed recent work on carbonyl complexes in detail with no mention of nitrosyl complexes. Another article on reactions of transition metal complexes (Niu, S.; Hall, M. B. *Chem. Rev.* **2000**, *100*, 353) explored the reactivity of the −NO ligand toward insertion into metal−carbon bonds formed by other ligands using B3LYP generated reaction profiles.
(52) Bauschlicher, C. W., Jr.; Siegbahn, P. E. M. *J. Chem. Phys.* **1986**, *85*, 2802.
(53) Williamson, R. L.; Hall, M. B. *Int. J. Quantum Chem. Quantum Chem. Symp.* **1987**, *21*, 503.
(54) Smith, S.; Hillier, I. H.; Von Niessen, W.; Guest, M. F. *Chem. Phys.* **1989**, *135*, 357.
(55) Fronzoni, G.; Decleva, P.; Lisini, A. *Chem. Phys.* **1993**, *174*, 57.
(56) Pedocchi, L.; Rovida, G.; Russo, N. *J. Electron. Spectrosc. Relat. Phenom.* **1994**, *69*, 81.
(57) Bohr, F.; Chermette, H.; Ruiz-Lopez, M. F. *Int. J. Quantum Chem.* **1994**, *52*, 1039.
(58) Darling, J. H.; Ogden, J. S. *J. Chem. Soc., Dalton Trans.* **1972**, 2496.
(59) Kushto, G. P.; Zhou, M. F.; Andrews, L.; Bauschlicher, C. W., Jr. *J. Phys. Chem. A* **1999**, *103*, 478.
(60) Krim, L.; Prot, C.; Alikhani, E. M.; Manceron, L. *Chem. Phys.* **2000**, *254*, 267.
(61) Vetter, R.; Naulin, C.; Costes, M. *Phys. Chem. Chem. Phys.* **2000**, *2*, 643.
(62) Kushto, G. P.; Andrews, L. *J. Phys. Chem. A* **1999**, *103*, 4836.
(63) Pyykkö, P.; Desclaux, J. P. *Chem. Phys. Lett.* **1977**, *50*, 503. Pyykkö, P. *Chem. Rev.* **1988**, *88*, 563. Chertihin, G. V.; Andrews, L. *J. Phys. Chem.* **1955**, *99*, 6356; *J. Am. Chem. Soc.* **1995**, *117*, 6402.
(64) Zhou, M. F.; Andrews, L. *J. Phys. Chem. A* **1999**, *103*, 478.
(65) Zhou, M. F.; Andrews, L. *J. Phys. Chem. A* **1998**, *102*, 10025.
(66) Andrews, L.; Wang, X. *J. Phys. Chem. A* **2002**, *106*, 1196.
(67) Zhou, M. F.; Andrews, L. *J. Phys. Chem. A* **2000**, *104*, 3915.
(68) Jacox, M. E. *Chem. Phys.* **1994**, *189*, 149.
(69) Andrews, L.; Zhou, M. F. *J. Phys. Chem. A* **1999**, *103*, 4167.
(70) Zhou, M. F.; Andrews, L. Unpublished results.
(71) Mitchell, S. A.; Hackett, P. A. *J. Chem. Phys.* **1990**, *93*, 7822.
(72) Andrews, L.; Chertihin, G. V.; Citra, A.; Neurock, M. *J. Phys. Chem.* **1996**, *100*, 11235.
(73) Fiedler, A.; Iwata, S. *J. Phys. Chem.* A **1998**, *102*, 3618.
(74) Citra, A.; Andrews, L. *J. Phys. Chem. A* **2000**, *104*, 8689. The BPW91 functional employed here gives essentially the same results as the BP86 functional: computed frequencies are generally within 10 $cm^{-1}$.
(75) Citra, A.; Andrews, L. *J. Phys. Chem. A* **2000**, *104*, 11897.
(76) Bauschlicher, C. W., Jr.; Bagus, P. S. *J. Chem. Phys.* **1984**, *80*, 944.
(77) Duarte, H. A.; Salahub, D. R. *J. Phys. Chem. B* **1997**, *101*, 7464.
(78) Alikhani, E. M.; Krim, L.; Manceron, L. *J. Phys. Chem. A* **2001**, *105*, 7817.
(79) Citra, A.; Andrews, L. *J. Phys. Chem. A* **2000**, *104*, 8160.
(80) Krim, L.; Alikhani, E. M.; Manceron, L. *J. Phys. Chem. A* **2001**, *105*, 7812.
(81) Smith, G. W.; Carter, E. A. *J. Phys. Chem.* **1991**, *95*, 2327.
(82) Knickelbein, M. B. *Annu. Rev. Phys. Chem.* **1999**, *50*, 79 and references therein.
(83) Rochefort, A.; Fournier, R. *J. Phys. Chem.* **1996**, *100*, 13506.
(84) Zhou, M. F.; Andrews, L. *J. Phys. Chem. A* **2000**, *104*, 2618.
(85) Manceron, L.; Krim, L.; Alikhani, E. A.; Wang, X.; Andrews, L. Unpublished results.
(86) Citra, A.; Andrews, L. *J. Phys. Chem. A* **2001**, *105*, 3042.
(87) Citra, A.; Wang, X.; Andrews, L. *J. Phys. Chem. A* ASAP Article JP010911a, Web Release Date July 24, 2001.
(88) Andrews, L.; Zhou, M. F.; Willson, S. P.; Kushto, G. P.; Snis, A.; Panas, I. *J. Chem. Phys.* **1998**, *109*, 177. Andrews, L.; Liang, B. *J. Am. Chem. Soc.* **2001**, *123*, 1997.
(89) Oriedo, J. V. B.; Russell, D. H. *J. Am. Chem. Soc.* **1993**, *115*, 8381.
(90) Sülzle, D.; Schwarz, H.; Moock, K. H.; Terlouw, J. K. *Int. J. Mass Spectrom. Ion Processes* **1991**, *108*, 269.
(91) Cassady, J. C.; Freiser, B. S. *J. Am. Chem. Soc.* **1985**, *107*, 1566.
(92) Khan, F. A.; Steele, D. L.; Armentrout, P. B. *J. Phys. Chem.* **1995**, *99*, 9, 7819.
(93) Zhou, M. F.; Andrews, L.; Bauschlicher, C. W., Jr. *Chem. Rev.* **2001**, *101*, 1931.
(94) Van Zee, R. J.; Weltner, W., Jr. *Chem. Phys. Lett.* **1997**, *266*, 403.
(95) Benjelloun, A. T.; Daoudi, A.; Berthier, G.; Rolando, C. *THEOCHEM* **1996**, *360*, 127.
(96) Goldman, A. S.; Krogh-Jespersen, K. *J. Am. Chem. Soc.* **1996**, *118*, 12159.
(97) Milligan, D. E.; Jacox, M. E. *J. Chem. Phys.* **1971**, *55*, 3404. Tevault, D. E.; Andrews, L. *J. Phys. Chem.* **1973**, *77*, 1640 and references therein.
(98) Kushto, G. P.; Ding, F.; Liang, B.; Wang, X.; Citra, A.; Andrews, L. *Chem. Phys.* **2000**, *257*, 223.
(99) Andrews, L.; Zhou, M.; Bare, W. D. *J. Phys. Chem. A* **1998**, *102*, 5019.
(100) Andrews, L.; Zhou, M. F.; Wang, X. *J. Phys. Chem. A* **2000**, *104*, 8475.
(101) Kay, J. G.; Green, D. W.; Duca, K.; Zimmerman, G. L. *J. Mol. Spectrosc.* **1989**, *138*, 49.
(102) Citra, A.; Andrews, L. *J. Phys. Chem. A* **2000**, *104*, 1152.
(103) Zhou, M.; Citra, A.; Liang, B.; Andrews, L. *J. Phys. Chem. A* **2000**, *104*, 3457.
(104) Willson, S. P.; Andrews, L. *J. Phys. Chem. A* **2000**, *104*, 3446.
(105) Windhorst, K. A.; Lunsford, J. H. *J. Am. Chem. Soc.* **1975**, *97*, 1407. Lundsford, J. H.; Hutta, P. J.; Lin, M. J.; Windhorst, K. A. *Inorg. Chem.* **1978**, *17*, 606.
(106) Jermyn, J. W.; Johnson, T. J.; Vansant, E. F.; Lunsford, J. H. *J. Phys. Chem.* **1973**, *77*, 2964. Yuen, S.; Chen. Y.; Kubsh, J. E.; Dumesic, J. A.; Topsoe, N.; Topsoe, H. *J. Phys. Chem.* **1982**, *86*, 3022.
(107) Sueiras, J. E.; Homs, N.; Ramirez de la Piscina, P.; Gracia, M.; Fierro, J. L. G. *J. Catal.* **1986**, *98*, 264. Rethwisch, D. G.; Dumesic, J. A. *J. Phys. Chem.* **1986**, *90*, 1625.
(108) Morrow, B. A.; Baraton, M. I.; Roustan, J. L. *J. Am. Chem. Soc.* **1987**, *109*, 7541.
(109) Johnston, C.; Jorgensen, N.; Rochester, C. H. *J. Chem. Soc., Faraday Trans.* **1988**, *84*, 2001.
(110) Aparicio, L. M.; Hall, W. K.; Fang, S. M.; Ulla, M. A.; Millman, W. S.; Dumesic, J. A. *J. Catal.* **1987**, *108*, 233.
(111) Shen, G. C.; Shido, T.; Ichikawa, M. *J. Phys. Chem.* **1996**, *100*, 16947.
(112) Naccache, C.; Ben Taarit, Y. *J. Chem. Soc., Faraday Trans. 2* **1973**, 1475.
(113) Valyon, J.; Hall, W. K. *J. Phys. Chem.* **1993**, *97*, 1204.
(114) Beutel, T.; Sarkany, J.; Lei, G. D.; Yan, J. Y.; Sachtler, W. M. H. *J. Phys. Chem.* **1996**, *100*, 845.
(115) Zhou, M. F.; Andrews, L. *J. Am. Chem. Soc.* **1999**, *121*, 9171.
(116) Erley, W. *Surf. Sci.* **1988**, *205*, L771.
(117) So, S. K.; Franchy, R.; Ho, W. *J. Chem. Phys.* **1991**, *95*, 1385.
(118) Brown, W. A.; Sharma, R. K.; King, D. A. *J. Phys. Chem. B* **1998**, *102*, 5303.
(119) Chen, P. J.; Goodman, D. W. *Surf. Sci.* **1993**, *297*, L93. Xu, X.; Chen, P.; Goodman, D. W. *J. Phys. Chem.* **1994**, *98*, 9242.
(120) Jigato, M. P.; Somasundram, K.; Termath, V.; Handy, N. C.; King, D. A. *Surf. Sci.* **1997**, *380*, 83.
(121) Avouris, Ph.; DiNardo, N. J.; Demuth, J. E. *J. Chem. Phys.* **1984**, *80*, 491.
(122) Davis, J. E.; Karseboom, S. G.; Nolan, P. D.; Mullins, C. B. *J. Chem. Phys.* **1996**, *105*, 8362.
(123) Gardner, P.; Martin, R.; Nalezinski, R.; Lamont, C. L. A.; Weaver, M. J.; Bradshaw, A. M. *J. Chem. Soc., Faraday Trans.* **1995**, *91*, 3575.
(124) Kao, C. T.; Blackman, G. S.; Van Hove, M. A.; Somorjai, G. A. *Surf. Sci.* **1989**, *224*, 77.
(125) Kim, Y. J.; Thevuthasan, S.; Herman, G. S.; Peden, C. H. F.; Chambers, S. A.; Belton, D. N.; Permana, H. *Surf. Sci.* **1996**, *359*, 269.
(126) For the trigonal $Cr(NO)_3^-$ example, BP86 gives N−O = 1.218 Å, $\nu_{antisym}$ = 1563.1 $cm^{-1}$ and BPW91 finds N−O = 1.216 Å, $\nu_{antisym}$ = 1537.5 $cm^{-1}$. For the $^3B_2$ $Cr(NO)_2$ example, BP86 gives N−O = 1.195 Å, $\nu_{antisym}$ = 1656.8 $cm^{-1}$ and BPW91 finds N−O = 1.193 Å, $\nu_{antisym}$ = 1663.5 $cm^{-1}$. For $^2\Delta$ FeNO, BP86 gives N−O = 1.186 Å, $\nu_{NO}$ = 1785.7 $cm^{-1}$ and BPW91 finds N−O = 1.186 Å, $\nu_{NO}$ = 1786.9 $cm^{-1}$. For $^2A'$ PtNO, BP86 gives N−O = 1.178 Å, $\nu_{NO}$ = 1711.2 $cm^{-1}$ and BPW91 finds N−O = 1.177 Å, $\nu_{NO}$ = 1717.6 $cm^{-1}$.


CR0000729